

Eastern Arabian Sea CO₂ outgassing during the Last Deglaciation and Holocene related to deep-water carbonate chemistry

Smita N. Naik^{1,2}, Sushant S. Naik^{1*}, Yair Rosenthal³ And Vincent Clementi³

¹CSIR-National Institute of Oceanography, Dona-Paula, Goa 403004, India

²School of Earth, Ocean and Atmospheric Sciences, Goa University, Goa, India

³Department of Marine and Coastal Sciences, Rutgers University,

*Corresponding author. e-mail: sushant@nio.org

Corresponding author: Sushant S. Naik

Abstract

Glacial to interglacial changes in atmospheric CO₂ are an intriguing part of carbon reorganization in the climate system and are estimated by investigating deep-water carbonate ion concentrations ([CO₃²⁻]). The scarcity of studies on [CO₃²⁻] in deep waters of the Indian Ocean and its role in the climate system inspired us to study the past carbonate ion variations from the eastern Arabian Sea (EAS). We analysed B/Ca ratios, δ¹³C, and δ¹⁸O of epibenthic foraminifera *Cibicidoides wuellerstorfi* from three cores bathing in different water masses of the EAS in order to determine deep-water [CO₃²⁻] and ventilation, spanning the Last Glacial Maximum (LGM) to the Holocene. This study reveals the existence of stored CO₂ in deep waters of the EAS during the LGM. We document two periods of rise in [CO₃²⁻] in deep waters, during the deglaciation and the mid-Holocene. The rise in [CO₃²⁻] during the deglaciation indicates outgassing of stored glacial CO₂ from deep waters via Southern Ocean and through escape via intermediate waters of the EAS. The minor rise in [CO₃²⁻] during the mid-Holocene could be due to release of CO₂ from deep water through upwelling, caused due to strengthening of southern hemisphere westerly winds since 5.3 ka.

Keywords: - Deep-water carbonate ion, benthic foraminifera, B/Ca, Arabian Sea, deglaciation, ventilation.

1. Introduction

The atmospheric CO₂ concentration has increased from 180 to ~280 ppmV from the last glacial maximum (LGM) to the late Holocene, respectively, and the oceans are implicated as the major control of this glacial-interglacial CO₂ change (Archer et al., 2000; Sigman and Boyle, 2000). The specific process underlying these variations is partially known, and is still debated. As the largest and yet responsive reservoir, the oceans control CO₂ gas in the atmosphere by drawing it in and out through its surface, depending upon its partial pressure relative to the atmosphere. Along with the biological uptake, CO₂ in oceans is taken up by dissolution of CO₂ in surface water, which increases the seawater alkalinity more than dissolved inorganic carbon (DIC) resulting in higher surface carbonate ion concentration. This process mostly occurs between 20-60° N latitude and intensively in the southern hemisphere (Takahashi et al., 2009). Thus, these parts of the global oceans act as a sink for atmospheric CO₂. Whereas, CO₂ is outsourced from the oceans through processes like intense upwelling, wherein the subsurface waters rich in nutrients and CO₂, upwells to the sea surface leading to an increase in partial pressure of CO₂ in surface water, thus exhaling CO₂ to the atmosphere. This exhaling of CO₂ mostly occurs in the tropical belt between 14° N to 14° S, wherein, the tropical Pacific is the largest source of CO₂ to atmosphere, whereas the Nordic Seas and parts of Arctic Seas in the North Atlantic are the largest sinks for CO₂ (Takahashi et al., 2009).

Today, the southern temperate Indian Ocean (14°-50° S) acts as a sink for atmospheric CO₂. Whereas, the region north of 14°N i.e. the north western Arabian Sea acts as source of CO₂ during peak upwelling time in the summer monsoon (June, July and August) due to high monsoon wind speed and higher *p*CO₂ in sub-surface waters (Takahashi et al., 2009), thus making the Arabian Sea a strong source of CO₂ to atmosphere second to the equatorial Pacific (Takahashi et al., 2002; Sarma et al., 2003). In-situ measurements using CTD carried out in the Arabian Sea during monsoon and intermonsoon seasons show that seawater *p*CO₂ is supersaturated with respect to the atmosphere for most part of the year and thus the AS is a perennial source of CO₂ to the atmosphere (Somasundar et al., 1990; George et al., 1994; Goyet et al., 1998; Sarma et al., 2003). Although the Arabian Sea acts as the source of CO₂, it is the western and the North Arabian Sea which majorly contribute to the emitted *p*CO₂ rather than the eastern Arabian Sea (EAS), which is affected by monsoonal precipitation. and the excessive influx of fresh water from precipitation and river runoff from the Western Ghats of India decreases the *p*CO₂ in surface waters. Hence the Arabian Sea shows a considerable spatial as well as seasonal contrast in *p*CO₂. A recent sub-annually resolved pH record (1990–2013) from the Arabian Sea based on δ¹¹B measurements on corals indicates significant inter-annual variations in pH (Tarique et al., 2022).

The spatial $p\text{CO}_2$ contrast in the Arabian Sea has also been maintained on the glacial to interglacial timescale as seen from $\delta^{11}\text{B}$ measurements in foraminifera from sediment cores. The western Arabian Sea (WAS) was seen to act as a constant source of CO_2 to atmosphere from 29 to 5 ka (Palmer et al., 2010), whereas, the EAS has acted as a persistent sink for atmospheric CO_2 for last 25 ka (Naik et al., 2015; Naik and Naik, 2018), except during the deglaciation, when the surface waters of the EAS showed a spike in $p\text{CO}_2$ signifying emission of CO_2 to the atmosphere during the period of 15 to 13 ka (Naik et al., 2015; Naik and Naik, 2018). Although the WAS constantly emitted CO_2 to atmosphere for the last 29 ka, its intensity was maximum during 14 to 11 ka interval (Palmer et al., 2010). A similar $p\text{CO}_2$ spike in surface waters of the west and east Equatorial Pacific (Palmer and Pearson, 2003; Martínez-Botí et al., 2015), south-west Pacific (Shao et al., 2019), Caribbean Sea (Foster, 2008), Equatorial and South Atlantic (Henehan et al., 2013; Martínez-Botí et al., 2015), North Atlantic (Ezat et al., 2017) and Southern Ocean (Moy et al., 2019; Shuttleworth et al., 2021) was also observed, indicating a global event, which is considered to be the cause of deglacial atmospheric CO_2 rise.

This CO_2 outgassing was widespread during the last deglaciation, reflected through the reconstructed $[\text{CO}_3]^{2-}$ at deeper depths, suggesting loss of carbon from the intermediate ocean to the atmosphere. Although the variation in $[\text{CO}_3^{2-}]$ has been studied in all the three major oceans of the world, there has been very small amount of work carried out in intermediate/deep waters of the Indian Ocean, one in the southwest Indian Ocean (Yu et al., 2010; Kerr et al., 2017) and other in the intermediate waters of the Arabian Sea and the Bay of Bengal (BoB; Ma et al., 2020), whereas, the deep waters of the Arabian Sea remain unexplored. In this study we use B/Ca ratios, carbon ($\delta^{13}\text{C}$) and oxygen ($\delta^{18}\text{O}$) stable isotopic ratio measurements in benthic foraminifera to unfold the variation in $[\text{CO}_3^{2-}]$ of deep waters of the southeast Arabian Sea, and assess their contribution to the rise in atmospheric CO_2 during the last deglaciation and Holocene and their relation to changes in ventilation.

2. Material and Methods

2.1 Study area

The Arabian Sea is highly dynamic in nature, with summer and winter monsoonal winds controlling the surface circulation by producing surface currents running in exactly opposite direction to each other, which in turn control upwelling and productivity in this region and show temporal and spatial heterogeneity. SW monsoon winds cause large-scale upwelling during summer in the western and northern Arabian Sea which increase productivity in the western Arabian Sea, and to a lesser extent in the EAS. In contrast, winter monsoon winds largely suppress upwelling in the west and north, but

result in moderate upwelling off Central India (Singh et al., 2011 and references therein). Higher biological production leads to reducing conditions in the intermediate layers thus necessitating denitrification while organic carbon is oxidised to CO₂. The Arabian Sea experiences an Oxygen Minimum Zone (OMZ) at a depth of 150-1200 meters (Wyrski, 1973; Naqvi, 1991) due to high biological productivity (Yentsch and Phinney, 1992; Banse and English, 1993) resulting from convective mixing in its north, during the northeast monsoon season (Madhupratap et al., 1996; Reichart et al., 1998).

The seasonal wind reversal greatly affects the CO₂ system in the surface waters of the Arabian Sea. The increased *p*CO₂ in surface waters of the AS mostly result from the upwelling and convective mixing of subsurface waters containing 1100 µatm of *p*CO₂ resulting from organic matter respiration (Sarma et al., 1998). However, a very small region of the EAS i.e. coastal waters at ~ 15° N shows low *p*CO₂ during southwest monsoon on account of high fresh water influx from small rivers in the Western Ghats which are highly active during summer monsoon (Sarma et al., 1998). Thus, physical processes control *p*CO₂ concentrations in surface waters during monsoon season, whereas, biological activities control *p*CO₂ during the inter-monsoon seasons (Sarma et al., 2000). Similarly, the EAS shows lower DIC as compared to western and northern Arabian Sea, due to influx of fresh waters from the Western Ghats and BoB during the southwest monsoon and northeast monsoon, respectively (Sarma et al., 2000).

The shallow to intermediate depth Arabian Sea is occupied by the following water masses: The Arabian Sea High Salinity Waters (ASHSW) are formed due to evaporative cooling of surface waters by cold/dry continental winds blowing over the Arabian Sea during winter monsoons. This water mass occupies the upper 150 m (Shetye et al., 1994; Prasanna Kumar and Prasad, 1999). The high salinity Persian Gulf Water (PGW) and Red Sea Water (RSW) masses occupy a depth of about 200-400 m and 500-800 m, respectively. The PGW and RSW water masses are bound by the Indian Central Water (ICW) (Emery and Meincke, 1986; Tomczak and Godfrey, 2003; Carton et al., 2012) along with contributions from Antarctic Intermediate Water (AAIW) and Indonesian Intermediate Water (IIW), both characterised by low salinities (Emery and Meincke, 1986; You and Tomczak, 1993). The AAIW lies below the thermocline throughout the subtropical Indian Ocean, and is the dominant water mass amongst the intermediate water masses of the Indian Ocean. It originates from deep convection of Sub-Antarctic Front in the southern hemisphere and can only be traced up to 5° N (You, 1998).

The Indian Ocean does not have any sources of deep or bottom water, but water parcels from the deepest layers originate from the ocean surface in the Atlantic and Southern Oceans. The Indian Deep Water (IDW) is the only deep-water mass formed within the Indian Ocean, by diffusion and

upwelling (Talley et al., 2011). The IDW is low in oxygen, and high in nutrients. Waters above 2000 m depth in the Indian Ocean have a net southward transport and those below 2000 m depth have a northward transport. The deep waters below 2000 m contain a high salinity core of the Circumpolar Deep Waters (CDW) / North Atlantic Deep Water (NADW), which is found south of 25°S, and a high salinity core of the IDW in the north. The CDW/ NADW has high oxygen and low silica. The Deep Western Boundary Currents (DWBCs) carry the CDW along each of the deep western boundaries of the Indian Ocean basins (Warren, 1974, 1978; Fieux et al., 1986; Johnson et al., 1991a, b; Warren and Johnson, 1992). There are two flow pathways from the south to the north Indian Ocean (Figure 1a), the western pathway through the Crozet and Madagascar Basins, along the Madagascar coast into the Somali and Arabian Basins. The eastern pathway is through the Southeast Indian Ridge into the South Australia Basin, and then through gaps in the Broken Plateau into the Central Indian and West Australia Basins. The NADW also enters directly from the South Atlantic without passing through the Antarctic Circumpolar Current (ACC). The bottom waters lying below the deep waters are the Lower Circumpolar Deep Water (LCDW), which is mainly the Antarctic Bottom Water (AABW), are colder, fresher, denser and high in oxygen. As the bottom waters circulate northward into the Indian Ocean they are modified due to diapycnal mixing, their aging reduces their oxygen content, and they acquire silica and nutrients (Talley et al., 2011). The densest waters are found in deep basins connected close to the Southern Ocean. However, they move northwards through gaps in the ridges and are warmer and less dense by the time they arrive in the northern Indian Ocean. The LCDW also upwells into the IDW.

2.2 Sediment cores

The three sediment cores for this study represent the different water masses in the Arabian Sea (Figure 1a and Table 1). Core AAS-9/21 was retrieved from a water depth of 1800 m from the EAS during A. A. Sidorenko cruise no. 9, and cores SK-129/CR-05 and SK-129/CR-02, were raised from the southeastern Arabian Sea from a depth of 2300 m and 3800 m, respectively during ORV Sagar Kanya cruise no. 129. The cores AAS-9/21 and SK-129/CR-05 lie well below the present day OMZ and above the Foraminiferal Lysocline (FL) depth of the Arabian Sea (FL= 3300 m; Cullen and Prell, 1984), except for core SK-129/CR-02, hence minimizing CaCO₃ dissolution at these depths. Cores SK-129/CR-05 and SK-129/CR-02, are presently bathed by the CDW entering the Indian Ocean and core AAS-9/21 is bathed by the HSDW. These cores lie in the flow path of southern sourced waters entering the Arabian Sea, making them appropriate core sites for investigating variations in deep-water [CO₃²⁻].

The $[\text{CO}_3^{2-}]$ distribution profile along the $\sim 68^\circ\text{E}$ transect, and between $\sim 5^\circ\text{S}$ and 17°N in the EAS (Figure 1b) shows low $[\text{CO}_3^{2-}]$ intermediate waters with slight increase in $[\text{CO}_3^{2-}]$ at deeper depths. The $[\text{CO}_3^{2-}]$ in the surface waters of Arabian Sea (Figure 1c) is higher, mostly due to photosynthetic activity, whereas lower $[\text{CO}_3^{2-}]$ at intermediate depths is due to the organic matter regeneration. Furthermore, an increase in $[\text{CO}_3^{2-}]$ at depths >1500 m is due to deep water ventilation from the South.

2.3 Age Model

The chronology of all the cores used in the study is based on radiocarbon (^{14}C) dates obtained by Accelerated Mass Spectrometer (AMS). Accelerated Mass Spectrometer ^{14}C dates were obtained on minimum of 13 mg of mixed species of *Globigerinoides sacculifer* and *Globigerinoides ruber* from a size range of 250-355 μm . Wherever the sample quantity was not adequate, *Neogloboquadrina dutertrei* was picked and added to obtain the desired quantity of sample. The chronology of core SK-129/CR-05 is based on seven AMS ^{14}C dates (Table 2) analysed at the Universität zu Köln, Germany. The foraminiferal samples were pre-treated with 1% HCl and washed with Milli-Q water of pH 6 prior to analyses. The chronology of core AAS-9/21 was adopted from Govil and Naidu, (2010) except for three additional dates which were obtained from the Universität zu Köln, Germany, to improve the chronology (Table 2; Naik and Naik, 2022). The age model for core SK-129/CR-02 was taken from Piotrowski et al., (2009). We have used an age-depth modelling routine named *Undatable*, which is developed in MATLAB and uses Bayesian radiocarbon (^{14}C) calibration software (MatCal) (Lougheed and Obrochta, 2019). These ^{14}C ages based age models were updated using Marine20 calibration data and a weighted mean $\Delta R = 42 \pm 54$ Downcore median ages, confidence intervals, and a density cloud that displays the most likely regions of age-depth probability were calculated by linearly interpolating all *nsim* (number of simulations) number of unique age-depth (Lougheed and Obrochta, 2019) runs to 1 depth unit resolution (e.g., cm), and then computing the 1st to 99th percentiles of the ages corresponding to each depth unit. Darker regions of the density cloud are closer to the 50th percentile. The age versus depth along with the uncertainties are provided (See supplementary figures 1 to 3).

2.4 Proxies

2.4.1 B/Ca

Boron/calcium analysis of benthic foraminifera was carried out on all the three cores, with minimum of 7 shells of *Cibicidoides wuellerstorfi* in the size range of 250-500 μm . Foraminiferal samples were partially crushed between two clean glass slides, transferred to acid cleaned vials, and

subjected to standard oxidative and reductive cleaning protocols to remove clay particles, organic matter, oxides, and adsorbed contaminants (Boyle and Keigwin, 1985, as modified in Rosenthal et. al., 1997). Cleaned samples were dissolved in ultrapure 0.065 N HNO₃ and analysed on a sector-field inductively coupled plasma mass spectrometer (ICP-MS, Thermo Scientific Element XR) at the Rutgers University. To improve washout efficiency and reduce boron memory effect between samples, anhydrous ammonia gas was injected into a high purity quartz cyclonic spray chamber, which raised the pH of the injected sample (>9.14, NBS scale; assessed by monitoring spray-chamber waste). This addition converts boric acid into soluble ammonium borate, which is more easily removed during wash out (Al-Ammar et al., 2000). The long term precision on B/Ca measurements, as determined by repeated analysis of consistency standards was ±3%, or an uncertainty of about ±2.5 µmol/kg (1 SD) on the [CO₃²⁻] estimates.

Contamination was identified by measuring Al/Ca, Fe/Ca and Mn/Ca ratios, and their covariance with B/Ca ratios was checked for all samples. The clay and silicate contamination was monitored by measuring the Al/Ca. The values of Al/Ca should be within 100 µmol/mol (Rae et al., 2011). In this study, Al/Ca ratios obtained for maximum samples were below 100 µmol/mol with no covariance of Al/Ca with B/Ca ratios. The contamination from Mn-Fe oxide coatings was checked by measuring Fe/Ca and Mn/Ca ratios and their values were below 100 µmol/mol and 1000 µmol/mol respectively (Barker et al., 2003). The Fe/Ca ratios did not show any covariance with B/Ca ratios, hence concluding an effective cleaning of foraminiferal shells. The Mn/Ca ratios were well below 1000 µmol/mol and showed a negative covariance with the B/Ca ratios, which again indicate efficient cleaning of shells.

The B/Ca ratios obtained from B/Ca analysis of *C. wuellerstorffi* shells were firstly converted to foraminiferal bottom water carbonate ion saturation ($\Delta[\text{CO}_3^{2-}]$) by using the correlation equation $[\text{B}/\text{Ca}] = 1.14 (\Delta[\text{CO}_3^{2-}]) + 176.6$ given by Yu and Elderfield (2007). Calcite saturation concentration ($[\text{CO}_3^{2-}]_{\text{sat}}$) was calculated using the CO₂sys.xls (Ver. 12) programme wherein the data of required parameters was taken from the Global Ocean Data Analysis Project (GLODAP) (Key et al., 2004). The constants used in programme are K₁ and K₂–Millero (2010), KSO₄ – Dickson (1990), B & Chlorinity - Lee et al. (2010) and pH in Total Scale. The down core in-situ carbonate ion concentrations ($[\text{CO}_3^{2-}]_{\text{in situ}}$) was obtained from the equation $[\text{CO}_3^{2-}]_{\text{in situ}} = \Delta[\text{CO}_3^{2-}] + [\text{CO}_3^{2-}]_{\text{sat}}$ which was then plotted against age.

2.4.2 Calcium carbonate (CaCO₃%)

Calcium carbonate analysis was carried out on core SK-129/CR-02 by taking about 2-3 mg of sample which was oven dried at 60°C for 24 hours and finely ground for analysis. The total inorganic

carbon (TIC) content was determined with a coulometer (UIC, Inc-CM140 acidification module) at the CSIR-National Institute of Oceanography, Goa. Analytical grade calcium carbonate was used as standard reference material. The precision of measurements was better than $\pm 2\%$ based on repeat analysis of laboratory standard after every 10 samples. The CaCO_3 weight percentage (%) was calculated by multiplying TIC with factor of 8.333. Calcium carbonate data for the cores AAS-9/21 and SK-129/CR-05 was taken from Godad et al., (2017) and Pattan et al., (2003) respectively.

2.4.3 Carbon and oxygen isotope analysis

Carbon and oxygen stable isotope analysis for core SK-129/CR-05 were done using minimum of two shells of benthic foraminifera *Cibicidoides wuellerstorfi* in the size range of 250-500 μm . The analysis was carried out on a KIEL IV device coupled to a Delta V IRMS at the CSIR-National Institute of Oceanography, Goa, India. The overall precision obtained was $\pm 0.04\text{‰}$ for $\delta^{13}\text{C}$ and $\pm 0.08\text{‰}$ for $\delta^{18}\text{O}$. Calibration to the VPDB standard was performed by repeated measurements of international reference standards NBS-19 and Carrara marble. Oxygen and carbon stable isotope data for core AAS-9/21 was taken from Naik and Naik, (2022), and the data for SK-129/CR-02 was adopted from Piotrowski et al. (2009).

3. Results

3.1 B/Ca and $[\text{CO}_3^{2-}]$

The B/Ca values in core AAS-9/21 range from 171 to 211 $\mu\text{mol/mol}$ which translate to a $[\text{CO}_3^{2-}]$ of 53 to 91 $\mu\text{mol/kg}$, for the last 25 ka (Figure 2a). During the LGM $[\text{CO}_3^{2-}]$ show a minimum value of 70 $\mu\text{mol/kg}$ at ~ 18 ka. Thereafter, an increase in $[\text{CO}_3^{2-}]$ is seen throughout the Heinrich Stadial 1 (HS1; ~ 17.5 to 14.7 ka) reaching a maximum of ~ 91 $\mu\text{mol/kg}$ during the Bølling-Allerød (BA; ~ 14.7 to 12.9 ka), which accounts for a 5.3 $\mu\text{mol/kg}$ rise during the deglaciation over the LGM, which is a significant increase based on a two-tailed Student's t test at a $> 90\%$ confidence level. Thereafter the $[\text{CO}_3^{2-}]$ sharply decreases during the latter part of the BA and remains low during the Younger Dryas (YD; ~ 12.9 to 11.7ka), and the Holocene. Again, the mid-Holocene shows a notable rise in $[\text{CO}_3^{2-}]$, which reaches a maximum of 75 $\mu\text{mol/kg}$ –at ~ 5 ka.

The B/Ca values in core SK-129/CR-05 range from 190 to 215 $\mu\text{mol/mol}$, which translate to a $[\text{CO}_3^{2-}]$ of 76 to 98 $\mu\text{mol/kg}$ over the last 25 ka (Figure 2b). The $[\text{CO}_3^{2-}]$ values show a large variability during the LGM and an average value of 88 $\mu\text{mol/kg}$. Further, a peak of 98 $\mu\text{mol/kg}$ is observed at ~ 15 ka during the HS1. A considerable gap in $[\text{CO}_3^{2-}]$ data exist between BA to mid Holocene, which is due to insufficient *C. wuellerstorfi* shells at those particular sections in the sediment core. The $[\text{CO}_3^{2-}]$

shows lower values during the Holocene than the deglaciation, reaching to a minimum of 76 $\mu\text{mol/kg}$ in the Late Holocene.

Core SK-129/CR-02 recorded B/Ca variations between 165 to 188 $\mu\text{mol/mol}$ over the last 25 ka, which in terms of $[\text{CO}_3^{2-}]$ is an 80 to 100 $\mu\text{mol/kg}$ variation (Figure 2c). The last glacial maximum shows comparatively lowered $[\text{CO}_3^{2-}]$ of ~ 90 $\mu\text{mol/kg}$ at a single available point. The $[\text{CO}_3^{2-}]$ peaked to ~ 100 $\mu\text{mol/kg}$ during the BA-YD. Thereafter, the $[\text{CO}_3^{2-}]$ shows a gradual decrease into the Holocene, which then increases in the mid-Holocene to 96 $\mu\text{mol/kg}$ at ~ 4 ka. The scarcity of data points in cores SK-129/CR-05 and 02 does not allow us to perform the Student's *t* test on these cores.

3.2 Calcium Carbonate Content ($\text{CaCO}_3\%$)

Calcium carbonate content in core SK-129/CR-02 (Figure 2c) varied between 49 to 69 % with highest values encountered during the YD. The CaCO_3 content showed lower values during the LGM compared to the deglaciation, which continued through the early HS1 and reached to minimum value of 49 % at ~ 16 ka. The values increased thereafter and reached a maximum of 68 % at ~ 11.5 ka, during the YD. A minor drop in values was observed thereafter, which then remained constant through the Holocene.

3.3 Carbon and oxygen isotope ratios in core SK-129/CR-05

The $\delta^{13}\text{C}$ values in core SK-129/CR-05 range from - 0.33 to 0.52 ‰ for last 25 ka (Figure 3a). Lowest values of - 0.33‰ were recorded in the LGM, whereas highest values of 0.52 ‰ were observed in the Holocene. The $\delta^{13}\text{C}$ values were near about similar during the LGM and HS1 with a slight decrease during the BA, followed by an increase in the YD to 0.18 ‰. The values then decreased during the early Holocene, and highest values were observed at the mid Holocene, which then decreased sharply in the late Holocene. Overall, the $\delta^{13}\text{C}$ values in this core showed an increasing trend from the LGM to the mid Holocene and a sharp decrease thereafter. The $\delta^{18}\text{O}$ values in core SK-129/CR-05 range from 1.79‰ at ~ 3 ka to 4.14 ‰ during the LGM (Figure 3b). The $\delta^{18}\text{O}$ values gradually dropped during the HS1, followed by a slight rise of 3.76 ‰ at ~ 15 ka in the BA, followed by a drop. The lowest $\delta^{18}\text{O}$ values were recorded in the Holocene with slight increase at ~ 2 ka in the Late Holocene. Overall, a decreasing trend in $\delta^{18}\text{O}$ values was seen from the LGM to Holocene.

4. Discussion

Carbonate ion concentration in seawater is affected by air-sea exchange, changes in alkalinity, CaCO_3 formation and dissolution at depth, organic carbon remineralisation, mixing of deep water masses and changes in deep-water circulation. Air-sea exchange occurs at the sea-surface wherein, due to the difference in the partial pressure, the CO_2 gas can either be taken up by seawater or given out to

the atmosphere. CO₂ evasion leads to lowering of DIC, which drives an increase in pH and shifts the carbonate equilibrium to the right, thus elevating [CO₃²⁻] of surface waters. A vice versa effect of CO₂ invasion occurs. Additionally, the temperature effect on [CO₃²⁻] is small at about 0.5 μmol/kg per °C and [CO₃²⁻] is insensitive to salinity changes (Yu et al., 2008). But, since the studied sediment cores lie at depths >1700 m, which represents deep-waters of the Arabian Sea, the changes occurring in [CO₃²⁻] due to air-sea exchange, temperature and salinity are insignificant. However, changes in alkalinity caused due to dissolution of calcium carbonate in deep-waters can drive up the [CO₃²⁻] in the water column. Every deep water mass has a unique preformed [CO₃²⁻], and biological effects on deep water masses are less significant, therefore, changes in deep-water circulation as well as the mixing of different water masses can play an important role in affecting [CO₃²⁻] of deep waters (Yu et al., 2008).

4.1 [CO₃²⁻] during the LGM

The average [CO₃²⁻] observed during the LGM is 76 μmol/kg, 87 μmol/kg, and 89 μmol/kg in cores AAS-9/21, SK-129/CR-05, and SK-129/CR-02 respectively (Figure 2a, 2b and 2c), and is lower as compared to the deglacial [CO₃²⁻] in all the three cores. The core AAS-9/21 (1800 m) showed the lowest [CO₃²⁻] in comparison to the deeper cores. A similar gradient of increasing [CO₃²⁻] with depth is evident in the modern ocean (Figure 1b and c). Low [CO₃²⁻] recorded during the LGM are consistent with lowered CaCO₃% (Figure 2a, b, c), and declined δ¹³C values in all the three cores (Figure 3a, 3c and 3d). Depleted δ¹³C values indicate lack of ventilation, higher nutrient concentration, and microbial organic matter respiration. Studies carried out using δ¹³C in the northern Indian Ocean showed δ¹³C-depleted and nutrient enriched water mass during the LGM, which could have resulted due to strong stratification/ poor ventilation of deep waters (Kallel et al., 1988; Ahmad et al., 2008; Piotrowski et al., 2009; Yu et al., 2010; Ma et al., 2019).

Organic carbon was sequestered in the deeper layers via the Southern Ocean by an enhanced biological pump, which transported high amounts of organic carbon to the global deep ocean during the LGM (Smetacek et al., 2012; Muglia et al., 2018; Rae et al., 2008). This organic carbon persisted in deep waters, accumulating respired CO₂, and the stratified deep waters further reduced its escape to mid-depths, yielding older and CO₂-rich deep waters (Skinner et al., 2010; Skinner et al., 2014; Skinner et al., 2017). The northward shift of the southern-hemisphere westerly wind belt and northward expansion of Antarctic sea ice led to reduced formation and/or overturning rate of southern-sourced water masses (i.e. AABW) and/or reduced air-sea CO₂ equilibration in the Southern Ocean during the LGM (Gottschalk et al., 2020). Thus the ventilation of the ocean interior was reduced. As a result large swaths of the Indian sector of the Southern Ocean accommodated an above-average share of the global-

ocean respired carbon at the LGM, largely contributing to the observed glacial reduction in $\text{CO}_{2,\text{atm}}$ (Gottschalk et al., 2020). The eastern Arabian Sea upwelling induced productivity was also higher in the glacial period due to stronger glacial winter monsoon winds (Singh et al., 2011), and similarly the equatorial Indian Ocean productivity was also high (Figure 3e; Yadav et al., 2022). Recent studies from the northern Indian Ocean also highlight the storage of CO_2 enriched deep-waters during the LGM (Bharti et al., 2022; Nisha et al., 2023). The observed poor ventilation during the last glaciation shows that the northern Indian Ocean was a part of the glacial ocean aged carbon pool (Nisha et al., 2023).

Sub-oxic conditions were observed in deep waters of the southeastern Arabian Sea (Sarkar et al., 1993; Pattan and Pearce, 2009), and the equatorial Indian Ocean during the LGM (Chandana et al., 2017), have been attributed to changes in deep-water circulation. Hence we had a look at the deep water circulation by observing the neodymium isotope (ϵ_{Nd}) record of deep waters of the Arabian Sea (Figure 3f, SK129, CR-05-Piotrowski et al., 2009; SK221-05-Lathika et al., 2021), and the BoB (Naik et al., 2019; Ma et al., 2019), which indicate decreased proportion of NADW reaching the northern Indian Ocean and the core sites, resulting in decreased ventilation of glacial deep waters. These two mechanisms, poor ventilation of deep waters, and increased surface productivity resulted in enhanced carbon respiration, which resulted in lowering of oxygen and $[\text{CO}_3^{2-}]$, and depletion of $\delta^{13}\text{C}$ of deep waters during the LGM, thus lowering $\text{CaCO}_3\%$ at our core sites.

4.2 The deglacial rise in $[\text{CO}_3^{2-}]$

A deglacial $[\text{CO}_3^{2-}]$ rise is seen in all the cores, beginning during the late Heinrich Stadial (HS1)/BA-YD (Figure 2a,b,c). However, the coarse resolution of our dataset could possibly explain the variable timing of the deglacial rise at these water depths. During the last deglaciation, pteropod preservation spikes were observed in the Andaman Sea (Sijinkumar et al., 2010; Sijinkumar et al., 2015), the Arabian Sea (Singh, 2007, Naidu et al., 2014) as well as a carbonate preservation spike across the northern Indian Ocean (Naik and Naidu, 2016), which signify better preservation at that time. These changes could have probably arisen through changes in circulation by an increased proportion of CO_3^{2-} -rich deep-waters at the core sites, degassing of CO_2 and upwelling in the Southern Ocean, and/or through in situ degassing of CO_2 from deep waters. The Atlantic meridional overturning circulation (AMOC) is thought to have been significantly reduced during HS1 and the YD as a result of freshwater input in the North Atlantic that prevented waters becoming dense enough to form deep waters (Vidal et al., 1997; McManus et al., 2004), and the NADW production was reduced. The North Atlantic Deep Waters are well oxygenated, nutrient-depleted, and contain highest $[\text{CO}_3^{2-}]$ of $\sim 125 \mu\text{mol/kg}$ (Broecker and Sutherland, 2000). At the end of HS1 the AMOC strengthened and NADW

production intensified. NADW being a well ventilated, carbonate rich water mass, which flowed northwards, flushed the deeper depths of the northern Indian Ocean. The CO₂ stored during the LGM, was released into the atmosphere by wind-driven upwelling of deep waters in the Southern Ocean during the deglaciation (Anderson et al., 2009; Skinner et al., 2010; Allen et al., 2015; Allen et al., 2020) thus contributing to the atmospheric CO₂ rise (Figure 4a). The fast increase in ¹⁴C and O₂ ventilation in the South Indian Ocean at the end of HS1, which is linked to a rapid resumption of Atlantic overturning, caused homogenization of the entire South Indian Ocean water column, laterally and vertically (Gottschalk et al., 2020). The ventilation age records from the northern Indian Ocean relate well to the Southern Ocean upwelling indices pointing towards the Southern Ocean as the source for redistribution of aged and intermediate water masses of the Southern Ocean (Nisha et al., 2023), which spread northward into the Pacific, Atlantic Ocean and Indian basin (Bryan et al., 2010). The upwelling of deep waters and reduction in Antarctic sea ice cover during the deglaciation caused substantial outgassing of CO₂ from the Southern Ocean, as recorded in the South Atlantic Ocean (Martínez-Botí et al., 2015; Shao et al., 2019; Shuttleworth et al., 2021), South Pacific Ocean (Allen et al., 2015, 2020; Moy et al., 2019; Allen et al., 2020; Shuttleworth et al., 2021) and the South Indian Ocean (Gottschalk et al., 2020; Ronge et al., 2020; Narayana et al., 2020), and contributed to an increase in atmospheric CO₂ of 80 ppmv. The outgassing of CO₂ from deep waters resulted in increased [CO₃²⁻] in deeper waters of the EAS as seen in this study and promoted better preservation of foraminiferal shells and CaCO₃ during the deglaciation. The Southern Ocean is said to thus play a significant role in sequestering as well as expelling stored deep-water carbon back to the surface layers in the Southern Ocean. An increased Southern Ocean ventilation and rise of atmospheric CO₂ noticed during the deglacial reveals their relation (Skinner et al., 2010).

The increase in [CO₃²⁻] is also observed at the water depth of 1800 m (AAS9/21; Figure 2a). During the NADW reduced phases of the HS1, an increased proportion of AAIW reached the northern Indian Ocean (Duplessy et al., 1984; Curry et al., 1988; Waelbroeck et al., 2006; Jung et al 2009; Romahn et al., 2014; Yu et al., 2018; Ma et al., 2019). However, the water depth of the shallowest core used in this study (AAS9/21) lies well below the depth of AAIW flow, and the AAIW is a water mass depleted in [CO₃²⁻]. Moreover, during the deglaciation, the AAIW carried old upwelled carbon from the Southern Ocean into the tropical Ocean's (See Marchitto et al., 2007). Hence AAIW is expected to have a lowered [CO₃²⁻], and its influence will rather lead to a [CO₃²⁻] decrease. Furthermore, the Persian Gulf being ~50 m deep was largely dry during the LGM. The Red Sea exchanges water with the Arabian Sea through the Bab el Mandeb which is currently having a sill depth of 130 m and had minimal water mass exchange during the LGM as the global drop in sea level was 120 m. Assuming

the initiation of sea level rise during the early deglaciation, the contribution of water masses from the Persian Gulf and Red Sea would have been minimum. Also, these water masses have low oxygen content, currently of 2.5-3 ml/l (Grasshoff, 1969; Wyrki et al., 1971), and are currently found in the Arabian Sea between a depth of 200–1000 m, where a severe and perennial OMZ is observed. The waters of the OMZ are not only oxygen depleted but also have high concentration of DIC (Paulmier et al., 2011), which signify low $[\text{CO}_3^{2-}]$. Hence, the minor proportions of water emerging from the OMZ also have low $[\text{CO}_3^{2-}]$ and thus mixing may not contribute to a rise in $[\text{CO}_3^{2-}]$ in core AAS-9/21 during the deglaciation. The core AAS-9/21 lies below the deep chemical front separating the intermediate and deep waters of the Arabian Sea (Kallel et al., 1988). The depth below 2000 m are dominated by the Indian Deep Water (IDW) (Talley et al., 2011), which has a significant proportion of the $[\text{CO}_3^{2-}]$ -rich-NADW. During the HS1, though the AMOC weakened, the NADW production did not fully halt, it rather was shallow (Skinner et al., 2021). It is hence possible that during the HS1, waters below the depth of 1800 m that had NADW contribution, were mixed vertically, thus increasing the $[\text{CO}_3^{2-}]$ at the water depth of AAS9/21. Later as the deglaciation progressed, the NADW production intensified and became the major contributor of waters to a depth between ~ 2000 m to 4000 m.

Along with CO_2 outgassing records from sites in the Southern Ocean, CO_2 outgassing was also observed at equatorial regions of the world oceans which includes the Equatorial Pacific (Palmer and Pearson, 2003; Martínez-Botí et al., 2015; Gray et al., 2018; Kubota et al., 2019), Atlantic (Foster and Sexton, 2014; Ezat et al., 2017) and the EAS (Naik et al., 2015, Figure 4b). The mechanism of CO_2 outgassing has been attributed to the excess CO_2 signal carried by the sub-Antarctic surface waters that are subducted in the sub-Antarctic Zone to form the AAIW, which is then transported to and upwelled at the equatorial regions of the major oceans. The ^{14}C and carbonate ion depleted AAIW during the deglaciation in the Southern Ocean (Basak et al., 2010) and its incursion in the Arabian Sea (Bryan et al., 2010; Ma et al., 2020) provides a major evidence for carrying the excess CO_2 to the Arabian Sea. The $[\text{CO}_3^{2-}]$ from the deeper Arabian Sea cores are comparable to another core from the southwest Indian Ocean, WIND 28K, retrieved from a water depth of 4147 m (Yu et al., 2010, Figure 4d), suggesting similar processes operating at these different locations. The elevated $[\text{CO}_3^{2-}]$ in deglacial deep waters is aligned in timing with the depleted ^{14}C signal in intermediate waters of the western Arabian Sea (Figure 4c, Bryan et. al., 2010), along with increased $p\text{CO}_2$ in surface waters of the EAS (Figure 4b, Palmer et al., 2010; Naik et al., 2015). The depleted ^{14}C signal is seen from the depth of ~3200 m to 1800 m suggesting the entire water column was ventilated during the deglaciation (Figure 4c). Other than the Southern Ocean loop, the CO_2 degassing may follow a direct path of escape from the deep to intermediate waters and to the atmosphere via surface waters of the Arabian Sea.

4.3 Variations in $[\text{CO}_3^{2-}]$ in the Holocene

Carbonate ion concentration in all the cores showed a decreasing trend through the Holocene. Closer examination of the Holocene $[\text{CO}_3^{2-}]$ in core AAS-9/21, SK-129/CR-05 and SK-129/CR-02 reveals a lowering of 18 $\mu\text{mol/kg}$, 9 $\mu\text{mol/kg}$ and 4.0 $\mu\text{mol/kg}$ respectively compared to the deglaciation. On the other hand, higher $\delta^{13}\text{C}$ values observed in some cores indicate well-ventilated and nutrient-depleted water mass like the NADW reaching the core sites, which was further confirmed from ϵ_{Nd} studies from the northern Indian Ocean (Piotrowski et al., 2009; Naik et al., 2019, Lathika et al., 2021). With increased proportion of NADW reaching the core sites, an elevated $[\text{CO}_3^{2-}]$ is expected. On the contrary, the decrease in $[\text{CO}_3^{2-}]$ can be attributed to the inter-basin carbonate compensation as suggested by Sosdian et al., (2018), which involves shifting of the calcium carbonate burial locus from the Atlantic Ocean basin to the Indo-Pacific Ocean basin. This mainly occurs through the changes in contribution of Antarctic Bottom Water/NADW during the cold/warm phases causes the dissolution/preservation of calcium carbonate in Atlantic sediments and this dissolution/preservation is balanced by the enhancing burial/ dissolution of calcium carbonate in the Indo-Pacific Ocean which causes preservation/dissolution of calcium carbonate during the glacial/interglacials. The whole mechanism of shifting of the locus of calcium carbonate preservation/dissolution mainly occurs through the changes in the $\Delta[\text{CO}_3^{2-}]$ of the deeper waters (Sosdian et al., 2018). Although the Indian Ocean behaved similar to the Atlantic Ocean during the LGM, it showed contrasting $[\text{CO}_3^{2-}]$ variations during the Holocene i.e. the $[\text{CO}_3^{2-}]$ values in deep waters of the Atlantic Ocean were seen to be increasing through the Holocene (Yu et al., 2008; Yu et al., 2010; Yu et al., 2014). The increased $[\text{CO}_3^{2-}]$ during the Holocene was mainly attributed to the replacement of $\delta^{13}\text{C}$ -depleted, low $[\text{CO}_3^{2-}]$ and corrosive southern sourced water mass by $\delta^{13}\text{C}$ -enriched, high $[\text{CO}_3^{2-}]$ NADW, due to the resumption of the AMOC (Yu et al., 2008; Yu et al., 2010; Yu et al., 2014). This burial of calcium carbonate is compensated by shifting of the locus of dissolution to the Indo-Pacific basin, causing dissolution of calcium carbonate during the Holocene. Hence, the Indian Ocean in terms of $[\text{CO}_3^{2-}]$ and preservation of CaCO_3 is corrosive and behaves similar to the Pacific Ocean today unlike the Atlantic Ocean.

Although a decrease in $[\text{CO}_3^{2-}]$ was observed throughout the Holocene, a minor rise was observed during the mid-Holocene at ~ 4 ka in all the cores, although not distinguishable in core SK129/CR-05 (Figure 2). This $[\text{CO}_3^{2-}]$ surge might have arisen on account of CO_2 outgassing of from deep waters to the atmosphere. A recent high-resolution study covering the last 8 ka discovered a $p\text{CO}_2$ spike in the surface waters of the northeast Arabian Sea thus demonstrating that the AS was a strong source of CO_2 to atmosphere from 5.5 to 4 ka (Azharuddin et al., 2022). This was attributed to the

strong ENSO activity, wherein frequent ENSO events resulted in intensification of the Findlater Jet (FLJ), which induced strong coastal upwelling by Kelvin waves and led to outgassing of CO₂. However, coastal upwelling caused due to intensification of FLJ and Kelvin waves is shallow. But since the cores used in this study lie at a depth of >1800 m, the upwelling of deep waters through such a process is questionable. Another possibility of a mid-Holocene rise in [CO₃²⁻] could be due to the strong upwelling of CO₂-rich CDW in the Antarctic zone, which can result in increased [CO₃²⁻] in deep waters as suggested by Moy et al. (2019). The strong upwelling in the Antarctic zone was caused due to constant and intense Southern Hemisphere westerly winds during 5.3-0 ka (Moreno et al., 2010; Saunders et al., 2018). This outsourcing of CO₂ via rise of pCO₂ in surface waters of the Southern Ocean was observed by Palmer and Pearson (2003); Moy et al. (2019); Shao et al. (2019); and Shuttleworth et al. (2021) in the Pacific Ocean during the Holocene.

To sum up, this study fills the data gap in Indian Ocean deep-water-[CO₃²⁻] studies. The Indian Ocean vertical [CO₃²⁻] profile, similar to the Pacific Ocean does not show much difference between the Holocene and LGM (Figure 5). The northern Indian Ocean [CO₃²⁻] lie between the Atlantic and Pacific values as expected owing to its intermediate location in the circulation pathway. The CO₃²⁻ water column gradient observed in the modern times (in situ measurements; Figure 1c) was maintained during the Holocene and the LGM (figure 5), implying efficient buffering of deep water pH by deep-sea CaCO₃ dissolution (Yu et al., 2014). The Holocene [CO₃²⁻] at 1800 m is the lowest amongst the global records as it lies just below an intense OMZ of the Arabian Sea (See Figure 1b). Future studies on [CO₃²⁻] from the OMZ-core can provide us clues on the mechanism hypothesised here on the escape of deep water CO₂ into intermediate waters and into the atmosphere, and also an understanding on [CO₃²⁻] variations in the OMZ through time.

5. Conclusion

This study highlights the importance of the northern Indian Ocean in deglacial atmospheric CO₂ rise. Low [CO₃²⁻] and δ¹³C values during the last glacial maximum indicate storage of CO₂ in deep waters of the Indian Ocean as observed in the Atlantic and Pacific Ocean. The rise in [CO₃²⁻] observed in all the three cores during the deglaciation is attributed to the outgassing of CO₂ from deep waters through upwelling in the Southern Ocean as a result of change in ocean circulation, and also via degassing of CO₂ from the eastern Arabian Sea. The variation in [CO₃²⁻] during the Holocene could be due to the inter-basin calcium carbonate compensation in response to changes in deep water circulation, as the [CO₃²⁻] in the Deep-Atlantic increased, which promoted CaCO₃ preservation in the Atlantic basin and dissolution in Indo-Pacific basin. In addition, rise in [CO₃²⁻] observed during the mid-Holocene could be due the outgassing of CO₂ from the Southern Ocean. The Indian Ocean vertical

[CO₃²⁻] profile is similar to the Pacific profile, with lowest [CO₃²⁻] recorded at ~ 1800 m water depth related to an overhead intense oxygen minimum zone.

Author Contributions: **Smita N. Naik:** Formal analysis, Investigation, Writing-Original Draft, Visualization **Sushant S. Naik:** Conceptualization, Resources, Writing - Review & Editing, Supervision, Project administration, Funding acquisition **Yair Rosenthal:** Methodology, Validation, Investigation, Resources, Writing - Review & Editing, Funding acquisition.

Declaration of competing interest: The authors declare that they have no known competing financial interests or personal relationships that could have appeared to influence the work reported in this paper.

Acknowledgements: We thank the director, CSIR-NIO for his support and permission to publish this work. This study was funded by the Extra Mural program funded by SERB (Deep-water carbonate chemistry of the northern Indian Ocean), sanction No. EMR/2016/000011 awarded to SSN. The CAF of CSIR-NIO is acknowledged for the IRMS facility. Anita Garg of NIO is acknowledged for the isotopic analysis and Vince Clementi of Rutgers, for age model calculations. This is CSIR-NIO contribution number XXXX.

References

- Ahmad, S. M., Babu, G. A., Padmakumari, V. M., Raza, W., 2008. Surface and deep water changes in the northeast Indian Ocean during the last 60 ka inferred from carbon and oxygen isotopes of planktonic and benthic foraminifera. *Palaeogeogr. Palaeoclimatol. Palaeoecol.* 262(3-4), 182-188. <https://doi.org/10.1016/j.palaeo.2008.03.007>.
- Al-Ammar, A., Reitznerová, E., Barnes, R., 2000. Determination of boron in biological samples. *J. Radioanal. Nucl. Chem. Artic.* 244(2), 267-272. <https://doi.org/10.1023/A:1006730013295>.
- Allen, K. A., Sikes, E. L., Hönisch, B., Elmore, A. C., Guilderson, T. P., Rosenthal, Y., Anderson, R. F., 2015. Southwest Pacific deep water carbonate chemistry linked to high southern latitude climate and atmospheric CO₂ during the Last Glacial Termination. *Quat. Sci. Rev.* 122, 180-191. <https://doi.org/10.1016/j.quascirev.2015.05.007>.
- Allen, K. A., Sikes, E. L., Anderson, R. F., Rosenthal, Y., 2020. Rapid loss of CO₂ from the south Pacific Ocean during the last glacial termination. *Paleoceanogr. Paleoclimatol.* 35(2), e2019PA003766. <https://doi.org/10.1029/2019PA003766>.
- Anderson, R. F., Ali, S., Bradtmiller, L. I., Nielsen, S. H. H., Fleisher, M. Q., Anderson, B. E., Burckle, L. H. 2009. Wind-driven upwelling in the Southern Ocean and the deglacial rise in atmospheric CO₂. *Science*, 323(5920), 1443-1448. <https://doi.org/10.1126/science.1167441>.
- Archer, D., Winguth, A., Lea, D., Mahowald, N., 2000. What caused the glacial/interglacial atmospheric pCO₂ cycles? *Rev. Geophys.* 38(2), 159-189. <https://doi.org/10.1029/1999RG000066>.

- Azharuddin, S., Govil, P., Chalk, T. B., Shekhar, M., Foster, G. L., Mishra, R., 2022. Abrupt upwelling and CO₂ outgassing episodes in the north-eastern Arabian Sea since mid-Holocene. *Sci. Rep.* 12(1), 1-12. <https://doi.org/10.1038/s41598-022-07774-4>.
- Banse, K., English, D. C., 1993. Revision of satellite-based phytoplankton pigment data from the Arabian Sea during the northeast monsoon. *Mar. Res.*, 2, 83-103.
- Barker, S., Greaves, M., Elderfield, H., 2003. A study of cleaning procedures used for foraminiferal Mg/Ca paleothermometry. *Geochem. Geophys. Geosys.* 4 (9). <https://doi.org/10.1029/2003GC000559>.
- Basak, C., Martin, E. E., Horikawa, K., Marchitto, T. M., 2010. Southern Ocean source of ¹⁴C - depleted carbon in the North Pacific Ocean during the last deglaciation. *Nat. Geosci.*, 3(11), 770-773. <https://doi:10.1038/ngeo987>.
- Boyle, E. A., Keigwin, L. D., 1985. Comparison of Atlantic and Pacific paleochemical records for the last 215,000 years: Changes in deep ocean circulation and chemical inventories. *Earth Planet. Sci. Lett.* 76(1-2), 135-150. [https://doi.org/10.1016/0012-821X\(85\)90154-2](https://doi.org/10.1016/0012-821X(85)90154-2).
- Broecker, W. S., Sutherland, S., 2000. Distribution of carbonate ion in the deep ocean: Support for a post Little Ice Age change in Southern Ocean ventilation? *Geochem. Geophys. Geosys.* 1 (7). <https://doi.org/10.1029/2000GC000039>.
- Bryan, S. P., Marchitto, T. M., Lehman, S. J., 2010. The release of ¹⁴C-depleted carbon from the deep ocean during the last deglaciation: Evidence from the Arabian Sea. *Earth Planet. Sci. Lett.* 298 (1-2), 244-254. <https://doi.org/10.1016/j.epsl.2010.08.025>.
- Carton, X., Hegaret, P., Baraille, R., 2012. Mesoscale variability of water masses in the Arabian Sea as revealed by ARGO floats. *Ocean Sci.* 8(2), 227-248. <https://doi.org/10.5194/os-8-227-2012>.
- Chandana, K. R., Bhushan, R., Jull, A. J. T., 2017. Evidence of poor bottom water ventilation during LGM in the equatorial Indian Ocean. *Front. Earth Sci.* 5, 84. <https://doi.org/10.3389/feart.2017.00084>.
- Cullen, J. L., Prell, W. L., 1984. Planktonic foraminifera of the northern Indian Ocean: distribution and preservation in surface sediments. *Mar. Micropaleontol.* 9(1), 1-52. [https://doi.org/10.1016/0377-8398\(84\)90022-7](https://doi.org/10.1016/0377-8398(84)90022-7).
- Curry, W. B., Duplessy, J. C., Labeyrie, L. D., Shackleton, N. J., 1988. Changes in the distribution of $\delta^{13}\text{C}$ of deep water ΣCO_2 between the last glaciation and the Holocene. *Paleoceanography* 3(3), 317-341. <https://doi.org/10.1029/PA003i003p00317>.
- Dickson, A. G., 1990. Standard potential of the reaction: $\text{AgCl(s)} + 1.2\text{H}_2(\text{g}) = \text{Ag(s)} + \text{HCl(aq)}$, and the standard acidity constant of the ion HSO_4^- in synthetic sea water from 273.15 to 318.15. *J. Chem. Thermodyn.* 22, 113-127. [https://doi:10.1016/00219614\(90\)90074-Z](https://doi:10.1016/00219614(90)90074-Z).
- Duplessy, J. C., Shackleton, N. J., Matthews, R. K., Prell, W., Ruddiman, W. F., Caralp, M., Hendy, C. H., 1984. ¹³C record of benthic foraminifera in the last interglacial ocean: implications for the carbon cycle and the global deep water circulation. *Quat. Res.* 21(2), 225-243. [https://doi.org/10.1016/0033-5894\(84\)90099-1](https://doi.org/10.1016/0033-5894(84)90099-1).

- Emery, W. J., Meincke, J. 1986. Global water masses-summary and review. *Oceanolo. Acta.* 9(4), 383-391.
- Ezat, M. M., Rasmussen, T. L., Hönisch, B., Groeneveld, J., Demenocal, P., 2017. Episodic release of CO₂ from the high-latitude North Atlantic Ocean during the last 135 kyr. *Nat. Commun.* 8(1), 1-10. <https://doi.org/10.1038/ncomms14498> (2017).
- Fieux, M., Schott, F., Swallow, J. C., 1986. Deep boundary currents in the western Indian Ocean revisited. *Deep Sea Res. Part I. Oceanogr. Res. Pap.* 33(4), 415-426. [https://doi.org/10.1016/0198-0149\(86\)90124-X](https://doi.org/10.1016/0198-0149(86)90124-X).
- Foster, G. L. 2008. Seawater pH, pCO₂ and [CO₃²⁻] variations in the Caribbean Sea over the last 130 kyr: A boron isotope and B/Ca study of planktic foraminifera. *Earth Planet. Sci. Lett.* 271(1-4), 254-266. <https://doi.org/10.1016/j.epsl.2008.04.015>.
- Foster, G. L., Sexton, P. F., 2014. Enhanced carbon dioxide outgassing from the eastern equatorial Atlantic during the last glacial. *Geology* 42(11), 1003-1006. <https://doi.org/10.1130/G35806.1>
- George, M. D., Kumar, M. D., Naqvi, S. W. A., Banerjee, S., Narvekar, P. V., De Sousa, S. N., Jayakumar, D. A., 1994. A study of the carbon dioxide system in the northern Indian Ocean during premonsoon. *Mar. Chem.* 47(3-4), 243-254. [https://doi.org/10.1016/0304-4203\(94\)90023-X](https://doi.org/10.1016/0304-4203(94)90023-X).
- GEOTRACES Intermediate Data Product Group (2021). The GEOTRACES Intermediate Data Product 2021 (IDP2021). NERC EDS British Oceanographic Data Centre NOC. DOI: [10.5285/cf2d9ba9-d51d-3b7c-e053-8486abc0f5fd](https://doi.org/10.5285/cf2d9ba9-d51d-3b7c-e053-8486abc0f5fd).
- Godad, S. P., Naik, S. S., Naidu, P. D., 2017. 70 kyr record of denitrification and oxygenation changes in the eastern Arabian Sea. *Geochem. J.* 51(4), 329-336. <https://doi.org/10.2343/geochemj.2.0472>.
- Gottschalk, J., Michel, E., Thöle, L. M., Studer, A. S., Hasenfratz, A. P., Schmid, N., Butzin, M., Mazaud A., Martinez-Gracia, A., Jaccard, S. L., 2020. Glacial heterogeneity in Southern Ocean carbon storage abated by fast South Indian deglacial carbon release. *Nat. Commun.* 11(1), 1-14. <https://doi.org/10.1038/s41467-020-20034-1>.
- Govil, P., Naidu, P. D., 2010. Evaporation precipitation changes in the eastern Arabian Sea for the last 68 ka: Implications on monsoon variability. *Paleoceanography*, 25, PA1210. <https://doi.org/10.1029/2008PA001687>.
- Goyet, C., Millero, F. J., O'Sullivan, D. W., Eischeid, G., McCue, S. J., Bellerby, R. G. J., 1998. Temporal variations of pCO₂ in surface seawater of the Arabian Sea in 1995. *Deep Sea Res. Part I: Oceanogr. Res. Pap.* 45(4-5), 609-623. [https://doi.org/10.1016/S0967-0637\(97\)00085-X](https://doi.org/10.1016/S0967-0637(97)00085-X).
- Grasshoff, K., 1969. Chemical observations in the Red Sea and the inner Gulf of Aden during the International Indian Ocean Expedition 1964/65. *Pangea*, <https://doi.org/10.1594/PANGAEA.603890>.
- Gray, W. R., Rae, J. W., Wills, R. C., Shevenell, A. E., Taylor, B., Burke, A., Foster, G. L., Lear, C. H., 2018. Deglacial upwelling, productivity and CO₂ outgassing in the North Pacific Ocean. *Nat. Geosci.* 11(5), 340-344. <https://doi.org/10.1038/s41561-018-0108-6>.

- Henehan, M. J., Rae, J. W., Foster, G. L., Erez, J., Prentice, K. C., Kucera, M., Bostock H. C., Martinez-Boti, M. A., Milton J. A., Wilson P. A., Marshall, J., Elliott, T. 2013. Calibration of the boron isotope proxy in the planktonic foraminifera *Globigerinoides ruber* for use in palaeo-CO₂ reconstruction. *Earth Planet. Sci. Lett.*, 364, 111-122. <https://doi.org/10.1016/j.epsl.2012.12.029>.
- Johnson, G. C., Warren, B. A., Olson, D. B., 1991a. Flow of bottom water in the Somali Basin. *Deep Sea Res. Part I. Oceanogr. Res. Pap.* 38(6), 637-652. [https://doi.org/10.1016/0198-0149\(91\)90003-X](https://doi.org/10.1016/0198-0149(91)90003-X).
- Johnson, G. C., Warren, B. A., Olson, D. B., 1991b. A deep boundary current in the Arabian Basin. *Deep Sea Res. Part I. Oceanogr. Res. Pap.* 38(6), 653-661. [https://doi.org/10.1016/0198-0149\(91\)90004-Y](https://doi.org/10.1016/0198-0149(91)90004-Y).
- Jung, S. J., Kroon, D., Ganssen, G., Peeters, F., Ganeshram, R., 2009. Enhanced Arabian Sea intermediate water flow during glacial North Atlantic cold phases. *Earth Planet. Sci. Lett.* 280(1-4), 220-228. <https://doi.org/10.1016/j.epsl.2009.01.037>.
- Kallel, N., Labeyrie, L. D., Juillet-Leclerc, A., Duplessy, J. C., 1988. A deep hydrological front between intermediate and deep-water, masses in the glacial Indian Ocean. *Nature*, 333(6174), 651-655. <https://doi.org/10.1038/333651a0>.
- Kerr, J., Rickaby, R., Yu, J., Elderfield, H., Sadekov, A. Y., 2017. The effect of ocean alkalinity and carbon transfer on deep-sea carbonate ion concentration during the past five glacial cycles. *Earth Planet. Sci. Lett.* 471, 42-53. <https://doi.org/10.1016/j.epsl.2017.04.042>.
- Key, R. M., Kozyr, A., Sabine, C. L., Lee, K., Wanninkhof, R., Bullister, J. L., Feely, R. A., Millero, F.J., Mordy, C., Peng, T. H., 2004. A global ocean carbon climatology: Results from Global Data Analysis Project (GLODAP). *Global Biogeochem. Cycles.* 18(4). <https://doi.org/10.1029/2004GB002247>.
- Kubota, K., Yokoyama, Y., Ishikawa, T., Sagawa, T., Ikehara, M., Yamazaki, T., 2019. Equatorial Pacific seawater pCO₂ variability since the last glacial period. *Sci. Rep.* 9(1), 1-11. <https://doi.org/10.1038/s41598-019-49739-0>
- Lathika, N., Rahaman, W., Tarique, M., Gandhi, N., Kumar, A., Thamban, M., 2021. Deep water circulation in the Arabian Sea during the last glacial cycle: Implications for paleo-redox condition, carbon sink and atmospheric CO₂ variability. *Quat. Sci. Rev.* 257, 106853. <https://doi.org/10.1016/j.quascirev.2021.106853>.
- Lee, K., Kim, T.-W., Byrne, R. H., Millero, F. J., Feely, R. A., Liu, Y.M., 2010. The universal ratio of boron to chlorinity for the North Pacific and North Atlantic oceans. *Geochim. Cosmochim. Acta.* 74(6), 1801–1811. <https://doi.org/10.1016/j.gca.2009.12.027>.
- Lougheed, B. C., Obrochta, S. P., 2019. A rapid, deterministic age-depth modelling routine for geological sequences with inherent depth uncertainty. *Paleoceanogr. Paleoclimatol.* 34, 122–133. <https://doi.org/10.1029/2018PA003457>.

- Ma, R., Sépulcre, S., Licari, L., Bassinot, F., Liu, Z., Tisnérat Laborde, N., Kallel, N., Yu, Z., Colin, C., 2019. Changes in intermediate circulation in the Bay of Bengal since the Last Glacial Maximum as inferred from benthic foraminifera assemblages and geochemical proxies. *Geochem., Geophys. Geosys.* 20(3), 1592-1608, <https://doi.org/10.1029/2018GC008179>.
- Ma, R., Sepulcre, S., Bassinot, F., Haurine, F., Tisnérat Laborde, N., Colin, C., 2020. North Indian Ocean Circulation Since the Last Deglaciation as Inferred From New Elemental Ratio Records for Benthic Foraminifera *Hoeglundina elegans*. *Paleoceanogr. Paleoclimatol.* 35(6), e2019PA003801. <https://doi.org/10.1029/2019PA003801>.
- Madhupratap, M., Kumar, S. P., Bhattathiri, P. M. A., Kumar, M. D., Raghukumar, S., Nair, K. K. C., Ramaiah, N. 1996. Mechanism of the biological response to winter cooling in the north eastern Arabian Sea. *Nature*, 384(6609), 549-552. <https://doi.org/10.1038/384549a0>.
- Martínez-Botí, M. A., Marino, G., Foster, G. L., Ziveri, P., Henehan, M. J., Rae, J. W., Mortyn P. G., & Vance, D. (2015). Boron isotope evidence for oceanic carbon dioxide leakage during the last deglaciation. *Nature*, 518(7538), 219-222. <https://doi.org/10.1038/nature14155>.
- McManus, J. F., Francois, R., Gherardi, J. M., Keigwin, L. D., Brown-Leger, S., 2004. Collapse and rapid resumption of Atlantic meridional circulation linked to deglacial climate changes. *Nature*, 428(6985), 834-837. <https://doi:10.1038/nature02494>.
- Millero, F. J., 2010. Carbonate constants for estuarine waters. *Mar. Freshw. Res.* 61, 139–142. <https://doi.org/10.1071/MF09254>.
- Moreno, P. I., Francois, J. P., Moy, C. M., Villa-Martínez, R., 2010. Covariability of the Southern Westerlies and atmospheric CO₂ during the Holocene. *Geology*, 38(8), 727-730. <https://doi.org/10.1130/G30962.1>
- Moy, A. D., Palmer, M. R., Howard, W. R., Bijma, J., Cooper, M. J., Calvo, E., Pelejero, C., Gagan, M. K., Chalk, T. B., 2019. Varied contribution of the Southern Ocean to deglacial atmospheric CO₂ rise. *Nature Geosci.* 12(12), 1006-1011. <https://doi.org/10.1038/s41561-019-0473-9>.
- Muglia, J., Skinner, L. C., Schmittner, A., 2018. Weak overturning circulation and high Southern Ocean nutrient utilization maximized glacial ocean carbon. *Earth Planet. Sci. Lett.*, 496, 47-56. <https://doi.org/10.1016/j.epsl.2018.05.038>.
- Naidu, P. D., Singh, A. D., Ganeshram, R., Bharti, S. K. 2014. Abrupt climate induced changes in carbonate burial in the Arabian Sea: Causes and consequences. *Geochem. Geophys. Geosys.* 15(4), 1398-1406. <https://doi.org/10.1002/2013GC005065>.
- Naik, S. S., Naidu, P. D., Foster, G. L., Martínez Botí, M. A., 2015. Tracing the strength of the southwest monsoon using boron isotopes in the eastern Arabian Sea. *Geophys. Res. Lett.* 42(5), 1450-1458. <https://doi.org/10.1002/2015GL063089>.
- Naik, S.S. Naidu, P.D., 2016. Carbonate preservation during the ‘mystery interval’ in the northern Indian Ocean. *Geochem. J.* 50, 357-362. <https://doi:10.2343/geochemj.2.0420>
- Naik, S. N., Naik, S. S., 2018. Evidences of CO₂ Leakage During the Last Deglaciation: The Need to Understand Deep-ocean Carbonate Chemistry of the Arabian Sea. *J. Geol. Soc. India*, 92(4), 404-406. <https://doi.org/10.1007/s12594-018-1034-3>.

- Naik, S. S., Basak, C., Goldstein, S. L., Naidu, P. D., Naik, S. N., 2019. A 16 kyr record of ocean circulation and monsoon intensification from the Central Bay of Bengal. *Geochem. Geophys. Geosys.*, 20(2), 872-882. <https://doi.org/10.1029/2018GC007860>.
- Naik, S. N., Naik, S. S. 2022. Glacial–interglacial contrast in deep-water $\delta^{13}\text{C}$ of the Arabian Sea. *J. Earth Syst. Sci.* 131(1), 1-10. <https://doi.org/10.1007/s12040-021-01796-8>
- Naqvi, W. A., 1991. Geographical extent of denitrification in the Arabian Sea in relation to some physical processes. *Oceanol. Acta.* 14 (3), 281-290. <https://archimer.ifremer.fr/doc/00101/21257/>.
- Narayana, A. C., Naidu, P. D., Bhavani, P. G., Ahmad, M., 2021. A coherent response of Southern Indian Ocean to the Antarctic climate: Implications to the lead, lags of atmospheric CO_2 during deglaciation. *J. Earth Syst. Sci.* 129(1), 1-8. <https://doi.org/10.1007/s12040-020-01484-z>.
- Nisha, K., Naik, S.S., Kumar, P., Banerjee, B., Rama Murty, P.B., 2023. Radiocarbon evidence for reduced deep water ventilation of the northern Indian Ocean during the last glacial maxima and early deglaciation. *Earth Planet. Sci. Lett.* 607, 118067, <https://doi.org/10.1016/j.epsl.2023.118067>.
- Palmer, M. R., Brummer, G. J., Cooper, M. J., Elderfield, H., Greaves, M. J., Reichart, G. J., Schouten, S., Yu, J. M., 2010. Multi-proxy reconstruction of surface water pCO_2 in the northern Arabian Sea since 29 ka. *Earth Planet. Sci. Lett.* 295(1-2), 49-57. <https://doi.org/10.1016/j.epsl.2010.03.023>
- Palmer, M. R., Pearson, P. N. 2003. A 23,000-year record of surface water pH and pCO_2 in the western equatorial Pacific Ocean. *Science*, 300(5618), 480-482. <https://doi.org/10.1126/science.1080796>.
- Paulmier, A., Ruiz-Pino, D., & Garçon, V. (2011). CO_2 maximum in the oxygen minimum zone (OMZ). *Biogeosciences*, 8(2), 239-252. <https://doi.org/10.5194/bg-8-239-2011>.
- Pattan, J. N., Masuzawa, T., Naidu, P. D., Parthiban, G., Yamamoto, M. 2003. Productivity fluctuations in the southeastern Arabian Sea during the last 140 ka. *Palaeogeogr. Palaeoclimatol. Palaeoecol.* 193(3-4), 575-590. [https://doi.org/10.1016/S0031-0182\(03\)00267-0](https://doi.org/10.1016/S0031-0182(03)00267-0).
- Pattan, J. N., Pearce, N. J. G., 2009. Bottom water oxygenation history in southeastern Arabian Sea during the past 140 ka: results from redox-sensitive elements. *Palaeogeogr. Palaeoclimatol. Palaeoecol.* 280(3-4), 396-405. <https://doi.org/10.1016/j.palaeo.2009.06.027>.
- Piotrowski, A. M., Banakar, V. K., Scrivner, A. E., Elderfield, H., Galy, A., Dennis, A., 2009. Indian Ocean circulation and productivity during the last glacial cycle. *Earth Planet. Sci. Lett.* 285(1-2), 179-189. <https://doi.org/10.1016/j.epsl.2009.06.007>.
- Prasanna Kumar, S., Prasad, T. G., 1999. Formation and spreading of Arabian Sea high salinity water mass. *J. Geophys. Res. Oceans* 104(C1), 1455-1464. <https://doi.org/10.1029/1998JC900022>.
- Reichart, G. J., Lourens, L. J., Zachariasse, W. J., 1998. Temporal variability in the northern Arabian Sea oxygen minimum zone (OMZ) during the last 225,000 years. *Paleoceanography* 13(6), 607-621. <https://doi.org/10.1029/98PA02203>.

- Romahn, S., Mackensen, A., Groeneveld, J., Pätzold, J., 2014. Deglacial intermediate water reorganization: New evidence from the Indian Ocean. *Clim. Past* 10(1), 293-303. <https://doi.org/10.5194/cpd-9-4035-2013>
- Ronge, T. A., Prange, M., Mollenhauer, G., Ellinghausen, M., Kuhn, G., Tiedemann, R., 2020. Radiocarbon evidence for the contribution of the Southern Indian Ocean to the evolution of atmospheric CO₂ over the last 32,000 years. *Paleoceanogr. Paleoclimatol.* 35(3), e2019PA003733. <https://doi.org/10.1029/2019PA003733>
- Ronge, T. A., Frische, M., Fietzke, J., Stephens, A. L., Bostock, H., Tiedemann, R., 2021. Southern Ocean contribution to both steps in deglacial atmospheric CO₂ rise. *Sci. Rep.*, 11(1), 1-10. <https://doi.org/10.1038/s41598-021-01657-w>.
- Rosenthal, Y., Boyle, E. A., Slowey, N., 1997. Temperature control on the incorporation of magnesium, strontium, fluorine, and cadmium into benthic foraminiferal shells from Little Bahama Bank: Prospects for thermocline paleoceanography. *Geochimi. Cosmochim. Acta* 61(17), 3633-3643. [https://doi.org/10.1016/S0016-7037\(97\)00181-6](https://doi.org/10.1016/S0016-7037(97)00181-6).
- Rae, J. W., Foster, G. L., Schmidt, D. N., Elliott, T., 2011. Boron isotopes and B/Ca in benthic foraminifera: Proxies for the deep ocean carbonate system. *Earth Planet Sci. Lett.* 302(3-4), 403-413. <https://doi.org/10.1016/j.epsl.2010.12.034>.
- Sarma, V. V. S. S., Kumar, M. D., George, M. D., 1998. The central and eastern Arabian Sea as a perennial source of atmospheric carbon dioxide. *Tellus B: Chem. Phys. Meteorol.* 50(2), 179-184. <https://doi.org/10.1034/j.1600-0889.1998.t01-1-00005.x>.
- Sarma, V. V. S. S., Kumar, M. D., Gauns, M., Madhupratap, M., 2000. Seasonal controls on surface pCO₂ in the central and eastern Arabian Sea. *J. Earth Syst. Sci.* 109(4), 471-479. <https://doi.org/10.1007/BF02708334>.
- Sarma, V. V. S. S., 2003. Monthly variability in surface pCO₂ and net air sea CO₂ flux in the Arabian Sea. *J. Geophys. Res. Oceans*, 108 (C8). <https://doi.org/10.1029/2001JC001062>.
- Sarkar, A., Bhattacharya, S. K., Sarin, M. M., 1993. Geochemical evidence for anoxic deep water in the Arabian Sea during the last glaciation. *Geochim. Cosmochim. Acta.* 57(5), 1009-1016. [https://doi.org/10.1016/0016-7037\(93\)90036-V](https://doi.org/10.1016/0016-7037(93)90036-V).
- Saunders, K. M., Roberts, S. J., Perren, B., Butz, C., Sime, L., Davies, S., Nieuwenhuyze, W. V., Grosjean, M., Hodgson, D. A., 2018. Holocene dynamics of the Southern Hemisphere westerly winds and possible links to CO₂ outgassing. *Nat. Geosci.* 11(9), 650-655. <https://doi.org/10.1038/s41561-018-0186-5>.
- Schlitzer, R., 2021. Ocean data view. <http://odv.awi.de>.
- Shao, J., Stott, L. D., Gray, W. R., Greenop, R., Pecher, I., Neil, H. L., Coffin, R. B., Davy, B., Rae, J. W., 2019. Atmosphere ocean CO₂ exchange across the last deglaciation from the Boron Isotope Proxy. *Paleoceanogr. Paleoclimatol.* 34(10), 1650-1670. <https://doi.org/10.1029/2018PA003498>.
- Shetye, S. R., Gouveia, A. D., Shenoi, S. S. C., 1994. Circulation and water masses of the Arabian Sea. *Proc. Indian Acad. Sci. Earth Planet. Sci.* 103(2), 107-123. <https://doi.org/10.1007/BF02839532>.

- Shuttleworth, R., Bostock, H. C., Chalk, T. B., Calvo, E., Jaccard, S. L., Pelejero, C., Martinez-Gracia, Foster, G. L., 2021. Early deglacial CO₂ release from the Sub-Antarctic Atlantic and Pacific oceans. *Earth Planet. Sci. Lett.* 554, 116649. <https://doi.org/10.1016/j.epsl.2020.116649>.
- Sigman, D. M., Boyle, E. A., 2000. Glacial/interglacial variations in atmospheric carbon dioxide. *Nature*, 407(6806), 859-869. <https://doi.org/10.1038/35038000>.
- Sijinkumar, A. V., Nath, B. N., Guptha, M. V. S., 2010. Late Quaternary record of pteropod preservation from the Andaman Sea. *Mar. Geol.* 275(1-4), 221-229. <https://doi.org/10.1016/j.margeo.2010.06.003>
- Sijinkumar, A. V., Nath, B. N., Guptha, M. V., Ahmad, S. M., Rao, B. R., 2015. Timing and preservation mechanism of deglacial pteropod spike from the Andaman Sea, north eastern Indian Ocean. *Boreas*, 44(2), 432-444. <https://doi.org/10.1111/bor.12099>
- Singh, A. D., 2007. Episodic preservation of pteropods in the eastern Arabian Sea: Monsoonal change, oxygen minimum zone intensity and aragonite compensation depth. *Indian J. Mar. Sci.* 36(4), 378-383. <http://nopr.niscpr.res.in/handle/123456789/69>.
- Skinner, L. C., Fallon, S., Waelbroeck, C., Michel, E., Barker, S., 2010. Ventilation of the deep Southern Ocean and deglacial CO₂ rise. *Science* 328(5982), 1147-1151. <https://doi:10.1126/science.1183627>.
- Skinner, L. C., Waelbroeck, C., Scrivner, A. E., Fallon, S. J., 2014. Radiocarbon evidence for alternating northern and southern sources of ventilation of the deep Atlantic carbon pool during the last deglaciation. *Proc. Natl. Acad. Sci. U.S.A.* 111(15), 5480-5484. <https://doi:10.1073/pnas.1400668111>.
- Skinner, L. C., Primeau, F., Freeman, E., de la Fuente, M., Goodwin, P. A., Gottschalk, J., Huang, E., McCave, I. N., Noble, T. L., Scrivner, A. E., 2017. Radiocarbon constraints on the glacial ocean circulation and its impact on atmospheric CO₂. *Nat. Commun.* 8(1), 1-10. <https://doi:10.17863/CAM.12351>.
- Skinner, L.C., Freeman, E., Hodell, D., Waelbroeck, C., Vazquez Riveiros, N., Scrivner, A.E., 2021. Atlantic Ocean Ventilation Changes Across the Last Deglaciation and Their Carbon Cycle Implications. *Paleoceanogr. Paleoclimatol.* 36, e2020PA004074. <https://doi.org/10.1029/2020PA004074>.
- Smetacek, V., Klaas, C. Strass, V. H., Assmy, P., Montresor, M., Cisewski, B., Savoye, N., Webb, A., d'Ovidio, F., Arrieta, J. M., Bathmann, U., Bellerby, R., Berg, G. M., Croot, P., Gonzalez, S., Henjes, J., Herndl, G. J., Hoffmann, L. J., Leach, H., Losch, M., Mills, M. M., Neill, C., Peeken, I., Röttgers, R., Sachs, O., Sauter, E., Schmidt, M. M., Schwarz, J. Terbruggen, A., Wolf-Gladrow, D., 2012. Deep carbon export from a Southern Ocean iron-fertilized diatom bloom, *Nature*, 47, 313-319. <https://doi:10.1038/nature11229>.
- Somasundar, K., Rajendran, A., Kumar, M. D., Gupta, R. S., 1990. Carbon and nitrogen budgets of the Arabian Sea. *Mar. Chem.* 30, 363-377. [https://doi.org/10.1016/0304-4203\(90\)90081-M](https://doi.org/10.1016/0304-4203(90)90081-M).

- Sosdian, S. M., Rosenthal, Y., Toggweiler, J. R., 2018, Deep Atlantic carbonate ion and CaCO₃ compensation during the Ice Ages, *Paleoceanogr. Paleoclimatol.* 33. <https://doi.org/10.1029/2017PA003312>.
- Takahashi, T., Sutherland, S. C., Sweeney, C., Poisson, A., Metzl, N., Tilbrook, B., Bates, N., Wanninkhofe, R., Feely, R. A., Sabine, C., Olafsson, J., Nojiri, Y., 2002. Global sea–air CO₂ flux based on climatological surface ocean pCO₂, and seasonal biological and temperature effects. *Deep Sea Res Part II: Top. Stu. Oceanogr.* 49(9-10), 1601-1622. [https://doi.org/10.1016/S0967-0645\(02\)00003-6](https://doi.org/10.1016/S0967-0645(02)00003-6).
- Takahashi, T., Sutherland, S. C., Wanninkhof, R., Sweeney, C., Feely, R. A., Chipman, D. W., Hales, B., Friederich, G., Chavez, F., Sabine, C., Watson, A., Bakker, D. C. E., Schuster, U., Metzl, N., Yoshikawa-Inoue, H., Ishii, M., Midorikawa, T., Nojiri, Y., De Baar, H. J., 2009. Climatological mean and decadal change in surface ocean pCO₂, and net sea–air CO₂ flux over the global oceans. *Deep Sea Res. Part II: Top. Stu. Oceanogr.* 56(8-10), 554-577. <https://doi.org/10.1016/j.dsr2.2008.12.009>.
- Talley et al. (2011) [Talley L.D., Pickard G.L., Emery W.J., Swift J.H., 2011. *Descriptive Physical Oceanography: An Introduction (Sixth Edition)*, Elsevier, Boston, 560 pp.]
- Tarique, M., Rahaman, W., A, F. A., N, L., Thamban, M., Achyuthan, H., Misra, S., 2021. Surface pH record (1990–2013) of the Arabian Sea from boron isotopes of Lakshadweep corals—trend, variability, and control. *J. of Geophys. Res.: Biogeosc.*, 126, e2020JG006122. <https://doi.org/10.1029/2020JG006122>
- Tomczak, M., Godfrey, J. S., 2003. *Regional oceanography: an introduction*. Daya books.
- Vidal, L., Labeyrie, L., Cortijo, E., Arnold, M., Duplessy, J. C., Michel, E., Becqué, S., Van Weering, T. C. E., 1997. Evidence for changes in the North Atlantic Deep Water linked to meltwater surges during the Heinrich events. *Earth Planet. Sci. Lett.* 146(1-2), 13-27. [https://doi.org/10.1016/S0012-821X\(96\)00192-6](https://doi.org/10.1016/S0012-821X(96)00192-6).
- Waelbroeck, C., Levi, C., Duplessy, J. C., Labeyrie, L., Michel, E., Cortijo, E., Bassinot, F., Guichard, F., 2006. Distant origin of circulation changes in the Indian Ocean during the last deglaciation. *Earth Planet. Sci. Lett.* 243(1-2), 244-251. <https://doi.org/10.1016/j.epsl.2005.12.031>.
- Warren, B. A., 1974. Deep flow in the Madagascar and Mascarene basins. *Deep-Sea Res. Oceanogr. Abstr.* 21 (1), 1-21. [https://doi.org/10.1016/0011-7471\(74\)90015-1](https://doi.org/10.1016/0011-7471(74)90015-1).
- Warren, B. A., 1978. Bottom water transport through the Southwest Indian Ridge. *DeepSea Res.*, 25(3), 315-321. [https://doi.org/10.1016/0146-6291\(78\)90596-9](https://doi.org/10.1016/0146-6291(78)90596-9).
- Warren, B. A., Johnson, G. C., 1992. Deep currents in the Arabian Sea in 1987. *Mar. Geol.*, 104, (1-4), 279-288. [https://doi.org/10.1016/0025-3227\(92\)90102-N](https://doi.org/10.1016/0025-3227(92)90102-N).
- Wyrtki, K., Bennett, E. B., Rochford, D. J., 1971. *Oceanographic atlas of the international Indian Ocean expedition (Vol. 531)*. Washington, DC: National Science Foundation.
- Wyrtki, K., 1973. An equatorial jet in the Indian Ocean. *Science*, 181(4096), 262-264. <https://doi.org/10.1126/science.181.4096.262>.

- Yentsch, C. S., Phinney, D.A., 1992. The effect of wind direction and velocity on the distribution of phytoplankton chlorophyll in the western Arabian Sea. In: *Oceanography of the Indian ocean.*, B.N. Desai, editor, Oxford & IBH, New Delhi, 57-66.
- You, Y., Tomczak, M., 1993. Thermocline circulation and ventilation in the Indian Ocean derived from water mass analysis. *Deep Sea Res. Part I: Oceanogr. Res. Pap.* 40(1), 13-56. [https://doi.org/10.1016/0967-0637\(93\)90052-5](https://doi.org/10.1016/0967-0637(93)90052-5).
- You, Y., 1998. Intermediate water circulation and ventilation of the Indian Ocean derived from water-mass contributions. *J. Mar. Res.* 56(5), 1029-1067. <https://doi.org/10.1357/002224098765173455>
- You, Y., 2000. Implications of the deep circulation and ventilation of the Indian Ocean on the renewal mechanism of North Atlantic Deep Water. *J. Geophys. Res. Oceans* 105(C10), 23895-23926. <https://doi.org/10.1029/2000JC900105>.
- Yu, J., Elderfield, H., 2007. Benthic foraminiferal B/Ca ratios reflect deep water carbonate saturation state. *Earth Planet. Sci. Lett.* 258(1-2), 73-86. <https://doi.org/10.1016/j.epsl.2007.03.025>.
- Yu, J., Elderfield, H., Piotrowski, A. M., 2008. Seawater carbonate ion- $\delta^{13}\text{C}$ systematics and application to glacial-interglacial North Atlantic Ocean circulation. *Earth Planet. Sci. Lett.* 271(1-4), 209-220. <https://doi.org/10.1016/j.epsl.2008.04.010>.
- Yu, J., Broecker, W. S., Elderfield, H., Jin, Z., McManus, J., Zhang, F., 2010. Loss of carbon from the deep sea since the Last Glacial Maximum. *Science* 330(6007), 1084-1087. <https://doi.org/10.1126/science.1193221>.
- Yu, J.M., Anderson, R.F., Jin, Z.D., Rae, J.W.B., Opdyke, B.N., Eggins, S.M., 2013. Responses of the deep ocean carbonate system to carbon reorganization during the Last Glacial-Interglacial cycle. *Quat. Sci. Rev.* 76, 39-52.
- Yu, J., Anderson, R. F., Rohling, E. J., 2014. Deep Ocean carbonate chemistry and glacial-interglacial atmospheric CO_2 changes. *Oceanography* 27(1), 16-25. <https://doi.org/10.5670/oceanog.2014.04>.
- Yu, Z., Colin, C., Ma, R., Meynadier, L., Wan, S., Wu, Q., Kallel, N., Sepulcre, S., Dapoigny, A., Bassinot, F., 2018. Antarctic Intermediate Water penetration into the Northern Indian Ocean during the last deglaciation. *Earth Planet. Sci. Lett.* 500, 67-75. <https://doi.org/10.1016/j.epsl.2018.08.006>.
- Yu, J., Menviel, L., Jin, Z. D., Thornalley, D. J., Foster, G. L., Rohling, E. J., McCave, I. N., McManus, J. F., Dai Y., Ren, H., He, F., Zhang, F., Chen, P.J., Roberts, A. P., 2019. More efficient North Atlantic carbon pump during the Last Glacial Maximum. *Nat. Commun.* 10 (1), 1-11. <https://doi:10.1038/s41467-019-10028-z>.

Legends to Figures

Figure 1a:- Map showing location of the cores used in the study, AAS-9/21, SK-129/CR-05 and SK-129/CR-02 (all shown as red circles). Black arrows indicate deep-water circulation in the Indian Ocean, essentially the flow paths of Circumpolar Deep Water (CDW) entering the Indian Ocean by two pathways, from southwest and southeast Indian Ocean. Thickness of the arrows refers to the intensity of the flow (You, 2000; Talley et al., 2011)

Figure 1b:- Image showing $[\text{CO}_3^{2-}]$ distribution profile along a transect (GI04) from the Eastern Arabian Sea (EAS), based on GEOTRACES data (GEOTRACES IDP 2021). Red circles in the profile indicate the three cores used for the study – AAS-9/21 (wd =1800 m), SK-129/CR-05 (wd =2300 m) and SK-129/CR-02 (wd =3800 m). This profile is generated using Ocean Data View (ODV, Schlitzer, 2021).

Figure 1c:- Vertical distribution of $[\text{CO}_3^{2-}]$ in the eastern Arabian Sea (EAS) (Station 944B-8.5°N & 71.2°E, GLODAP; Key et al., 2004). The red line shows the calcite saturation curve. The calcite saturation horizon (marked in grey line) is the depth where in-situ $[\text{CO}_3^{2-}] = [\text{CO}_3^{2-}]$ saturation.

Figure 2:- Graph showing variations in B/Ca ($\mu\text{mol/kg}$), $[\text{CO}_3^{2-}]$ ($\mu\text{mol/kg}$), and CaCO_3 (%) in cores a) AAS-9/21 (red circles, water depth = 1800 m) b) SK-129/CR-05 (green circles, water depth = 2300 m), and c) SK-129/CR-02 (blue circles, water depth = 3800 m). Grey open circles depict variation in CaCO_3 (%) in the respective cores. The CaCO_3 (%) data in core AAS-9/21 and SK-129/CR-05 is taken from Godad et al., 2017 and Pattan et al., 2003, respectively. Grey bands in the figure indicate Heinrich Stadial 1 (HS1) and Younger Dryas (YD). White band indicates the Bølling-Ållerød (BA). The Last Glacial Maximum (LGM), deglaciation and Holocene are marked with arrows on the top axis and dotted lines.

Figure 3:- Graph showing variations in a) $\delta^{13}\text{C}$ of *C. wullerstorfi* in core SK-129/CR-05 (green squares) b) $\delta^{18}\text{O}$ of *C. wullerstorfi* in core SK-129/CR-05 (orange squares) (The precision obtained was $\pm 0.04\%$ for $\delta^{13}\text{C}$, and $\pm 0.08\%$ for $\delta^{18}\text{O}$), c) $\delta^{13}\text{C}$ of *C. wullerstorfi* in core AAS-9/21 (red squares; Naik and Naik, 2022), d) $\delta^{13}\text{C}$ of *C. wullerstorfi* in core SK-129/CR-02 (blue squares; Banakar et al., 2005), e) ϵ_{Nd} in core SK-129/CR-02 (pink squares; Piotrowski et al., 2009), and core SK221-05 (purple squares, 9°N, 72.09°E, water depth = 2700; Lathika et al., 2021) and, f) Ratio of mixed layer eutrophic species (MLES = *G. bulloides* and *G. glutinata*) to mixed layer oligotrophic species (MLOS = *G. ruber*, *G. sacculifer*, *G. quadrilobatus* and *G. triloba*) in core SSD-044/GC-01. An increased ratio suggests increased productivity (yellow squares, 5°N, 77°E, water depth = 3160 m; Yadav et al., 2021). Grey bands in the figure indicate Heinrich Stadial 1 (HS1) and Younger Dryas (YD). White band indicates the Bølling-Ållerød (BA). The Last Glacial Maximum (LGM), deglaciation and Holocene are marked with arrows on the top axis and dotted lines.

Figure 4:- Graph showing variations in a) atmospheric CO_2 (orange open circles; Bazin et al., 2013), b) surface water $p\text{CO}_2$ in core AAS-9/21 (purple squares; Naik et al., 2015), c) ventilation ages of the core SSD-044/GC-01 (blue triangles; water depth = 3160 m; Nisha et al., 2023), core RC27-23 (orange circles, 18°N, 57.6°E, water depth = 820 m; Bryan et al., 2010), and core SS152/3828 (black squares, 3.89°N, 78.06°E, water depth = 3166 m; Bharti et al., 2022). These ventilation ages are the benthic-planktic radiocarbon age differences, e) variations in deep-water $[\text{CO}_3^{2-}]$ in the Indian Ocean, WIND 28 K (black line, water depth =4257 m; Yu et al., 2010), SK-129/CR-02 (blue squares, this study), SK-129/CR-05 (green squares, this study) and AAS-9/21 (red squares, this study). Grey bands in the figure indicate Heinrich Stadial 1 (HS1) and Younger Dryas (YD). White bands indicate the Bølling-Ållerød (BA). The Last Glacial Maximum (LGM), deglaciation and Holocene are marked with arrows on the top axis and dotted lines.

Figure 5:- Vertical profiles of carbonate ion concentration [CO_3^{2-}] for the LGM and Late Holocene reconstructed from B/Ca. Purple stars represent averages from this study between 0 and 5 ka (filled symbol) and 18 and 24 ka (open symbol). Blue and pink symbols are data that have been previously published (Yu et al., 2008; Yu et al., 2013; Allen et al., 2015). Horizontal bars represent 1-sigma uncertainty of the mean.

Legends to Tables

Table 1:- Sediment cores used in this study with core IDs, location and water depth.

Table 2:- AMS radiocarbon ages for core SK-129/CR-05.*the model output of calibrated age at each cm interval along with the uncertainties is provided in the supplementary material.

Table 3:- Average deep water [CO_3^{2-}] for selected time intervals at the three studied sites. Errors represent 1 standard deviation (1σ) of reconstructions within the indicated time interval.

Figure 1a

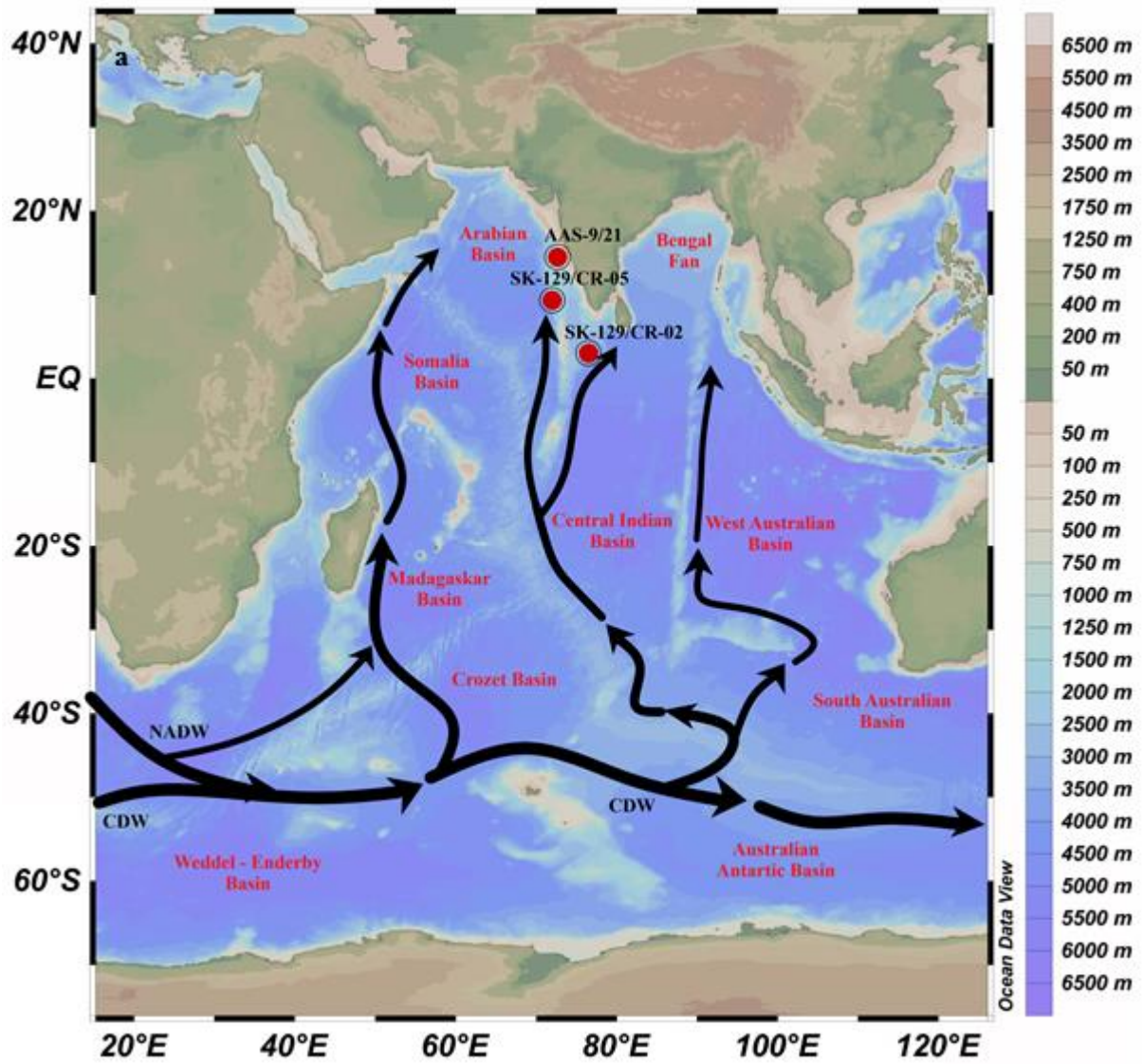


Figure 1b

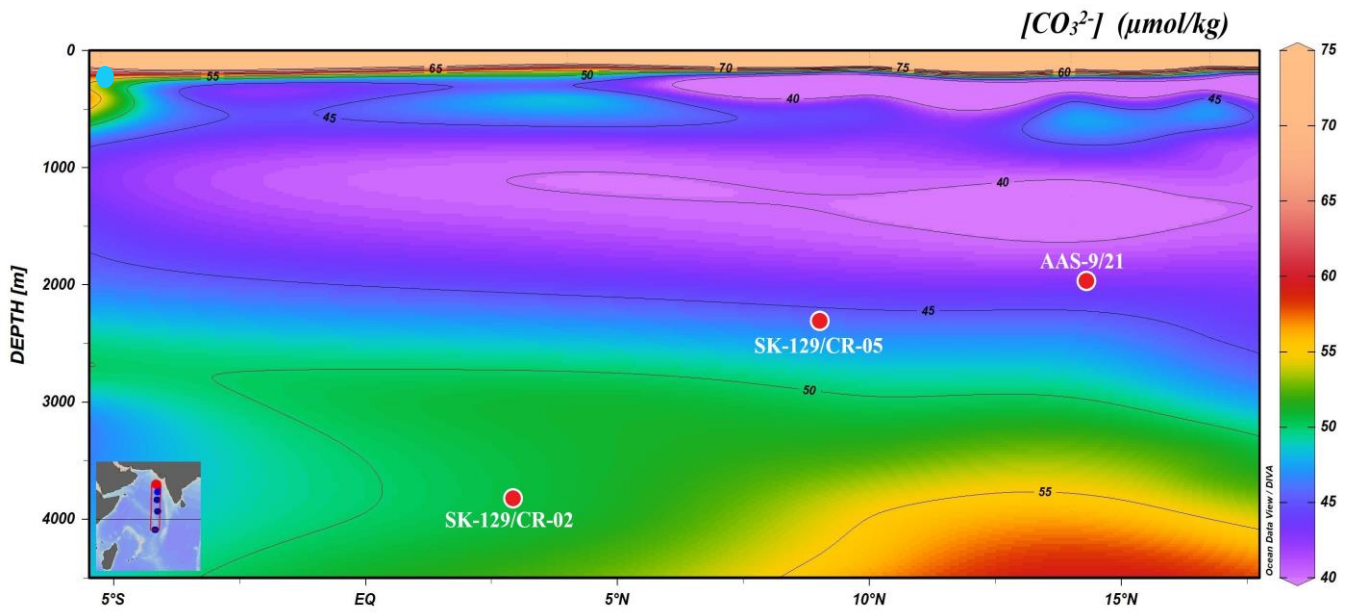


Figure 1c

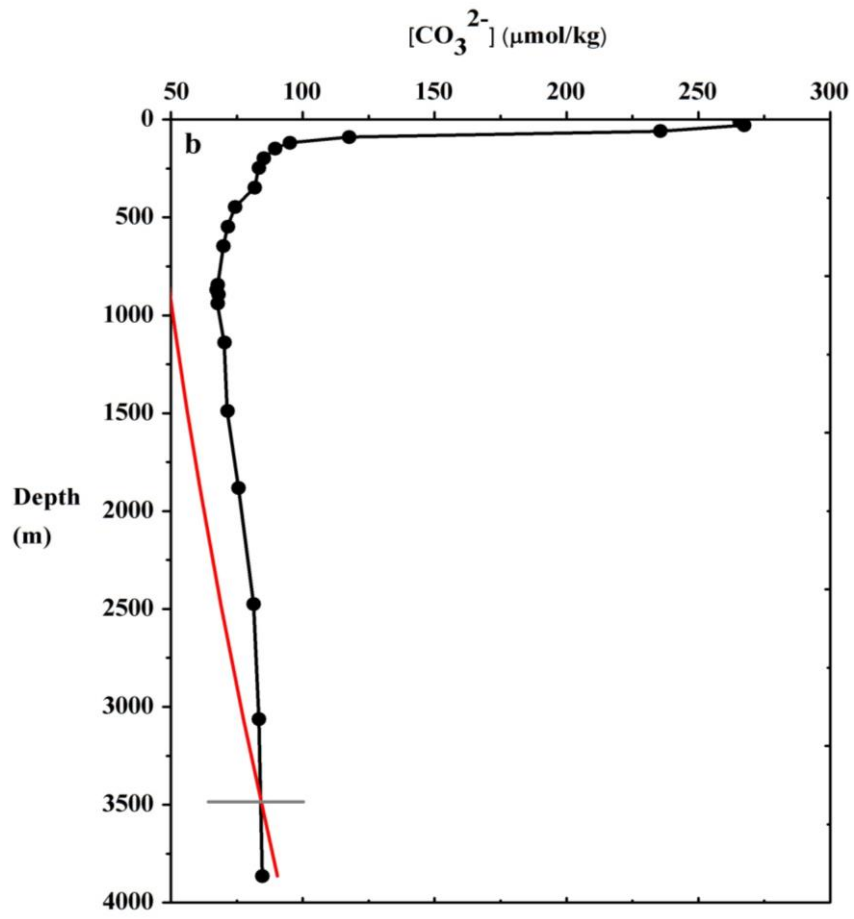
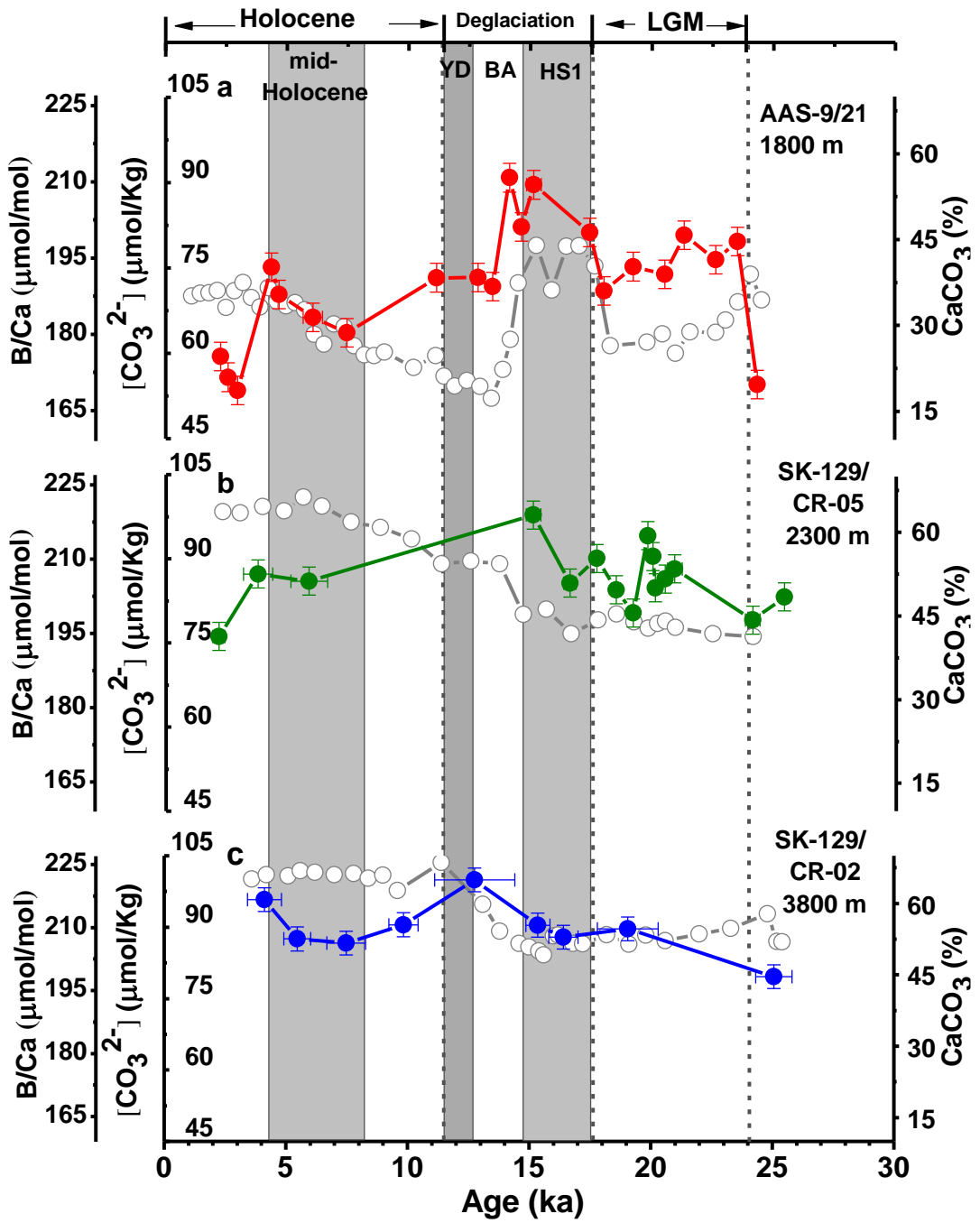


Figure 2



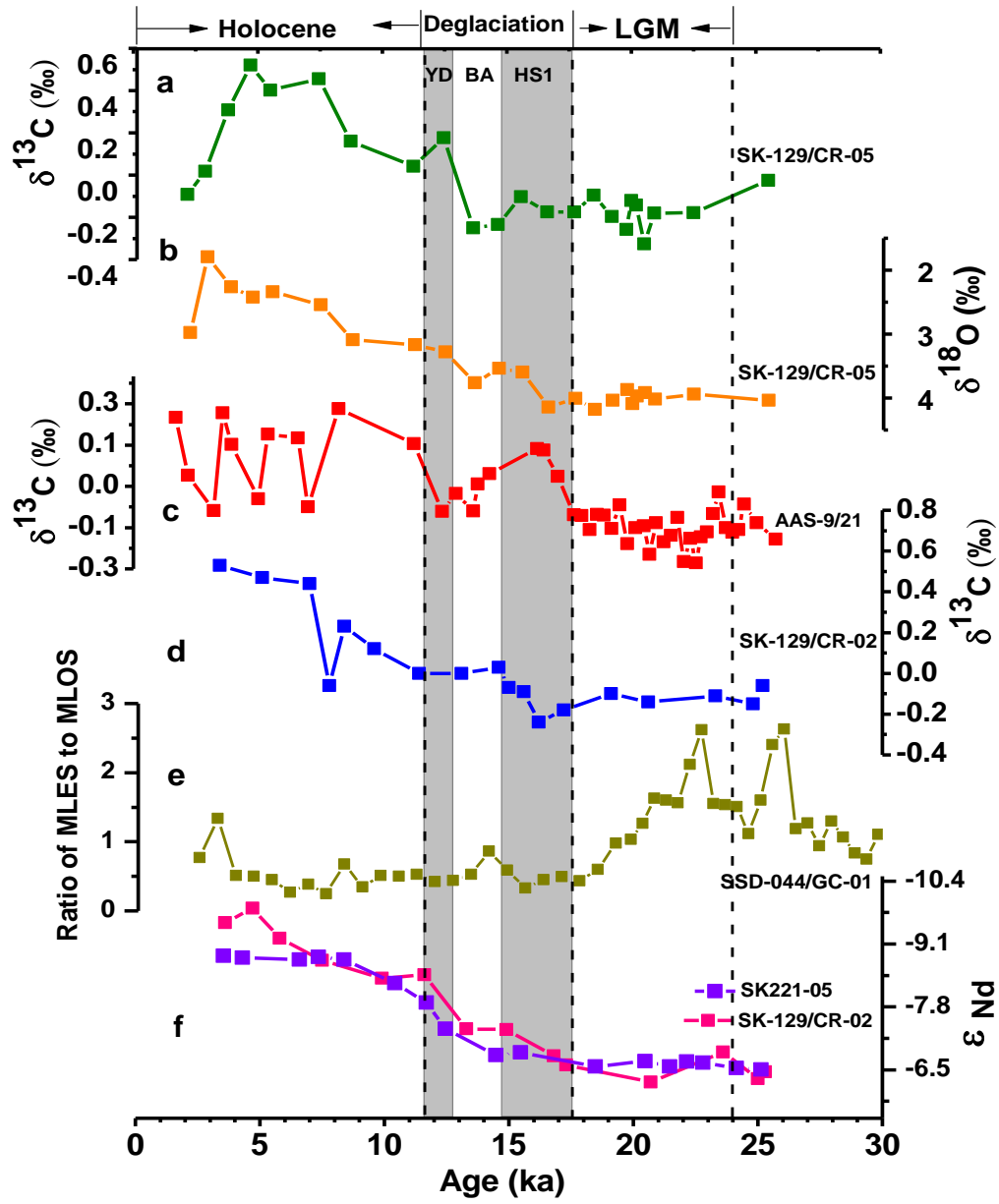


Figure 3

Figure 4

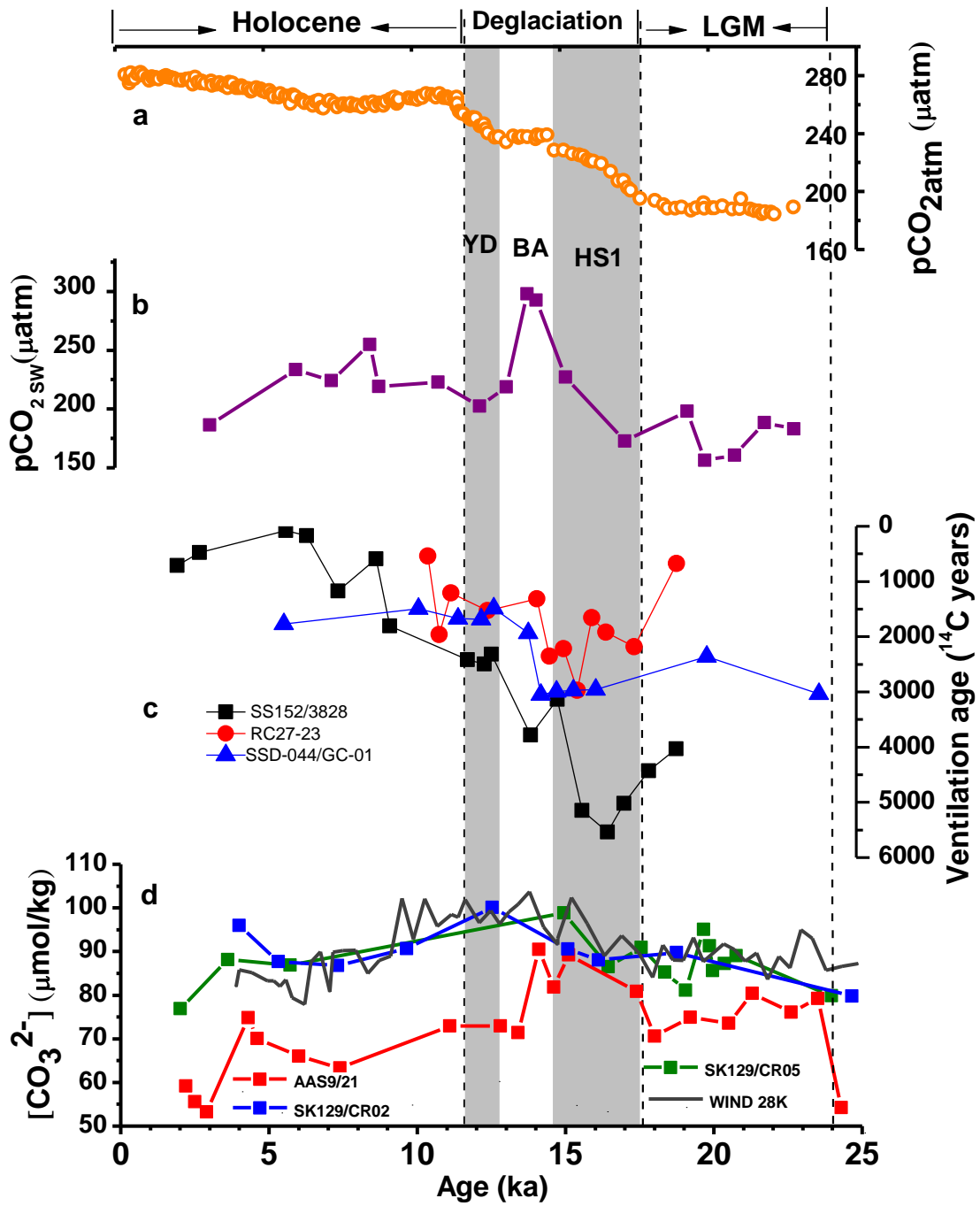


Figure 5

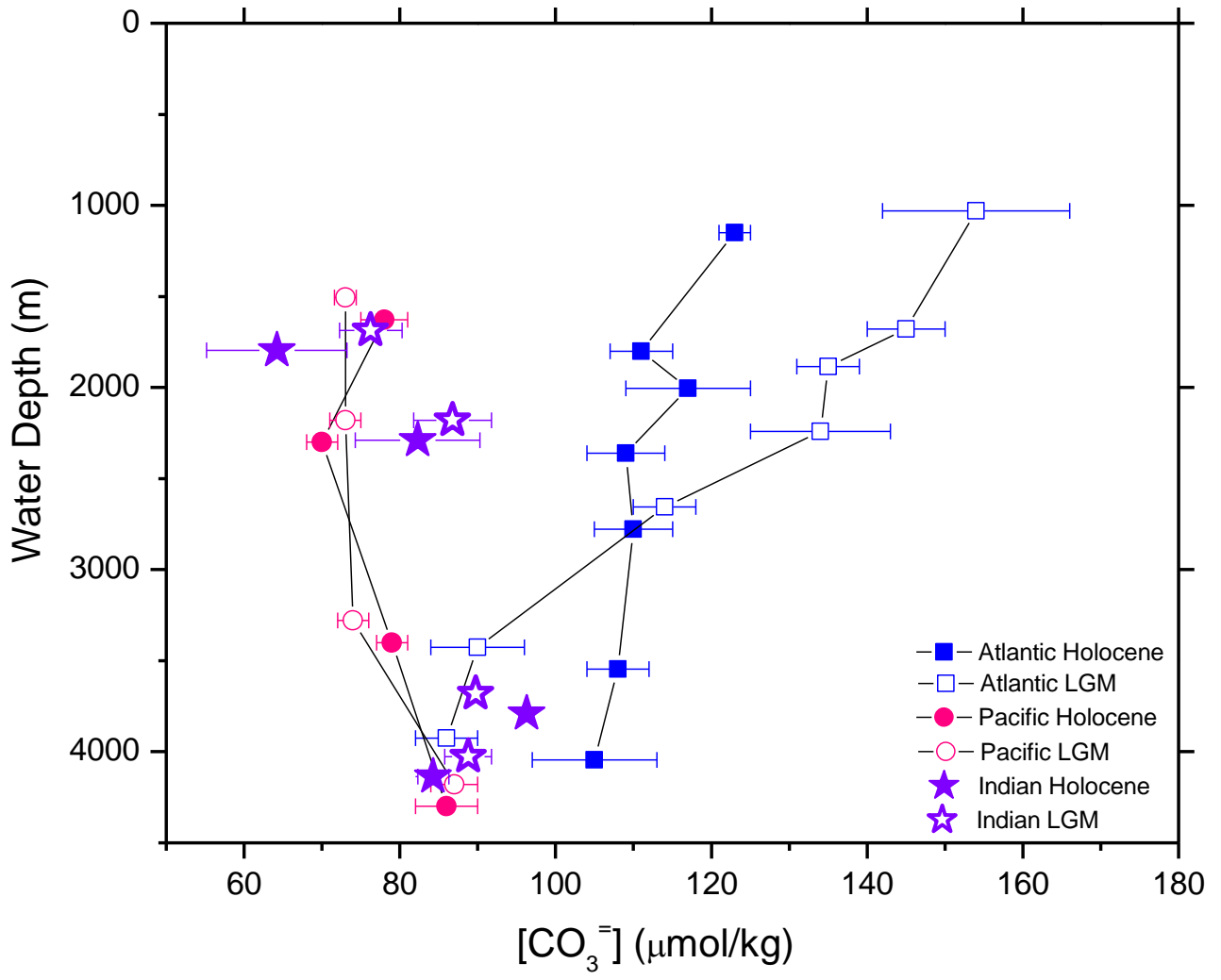


Table 1

Sr. No.	Core ID	Latitude	Longitude	Water Depth (m)
1	AAS-9/21	14.50° N	72.65° E	1800
2	SK-129/CR-05	9.35° N	71.98° E	2300
3	SK-129/CR-02	3.02° N	76.50° E	3800

Table 2

Sr. No.	AMS-Lab-ID	SK-129/CR-05 sample interval (cm)	F ¹⁴ C±%	¹⁴ C age (yr BP)	Species used
1	COL5308	0-4	0.711±0.32	2743±25	<i>G. sacculifer</i>
2	COL5309	22-24	0.460±0.36	6240±29	<i>G. sacculifer</i>
3	COL5310	46-48	0.208±0.48	12598±39	<i>G. sacculifer</i>
4	COL5311	62-64	0.142±0.61	15654±49	<i>G. sacculifer, G.ruber</i>
5	COL5312	70-72	0.122±0.77	16910±62	<i>G. sacculifer, G.ruber, N. dutertrei</i>
6	COL5313	86-88	0.106±0.74	18042±59	<i>G. sacculifer, G.ruber</i>
7	COL5314	98-100	0.061±0.82	22434±66	<i>G. sacculifer, G.ruber</i>
Sr. No.	AMS-Lab-ID	AAS-9/21 sample interval (cm)		¹⁴ C age (yr BP)	Species used
1	COL5315	96-99	0.216±0.42	13546±33	<i>G. sacculifer, G.ruber</i>
2	COL5316	116-119	0.190±0.45	13326±36	<i>G. sacculifer, G.ruber</i>
3	COL5317	136-139	0.155±0.48	14953±39	<i>G. sacculifer, G.ruber</i>

Table 3

Sr. No.	Core	Deep water [CO ₃ ²⁻]	
		Late Hol (0-5)	LGM (18-24)
1	AAS-9/21	64 ± 9 (5) ^a	76 ± 4 (7)
2	SK-129/CR-05	82 ± 8 (2)	87 ± 5 (9)
3	SK-129-CR-02	96 (1)	90 (1)

^anumber of samples used for averaging